

A joint spatiotemporal model for multiple longitudinal markers and competing events

Juliette ORTHOLAND* | Stanley DURRLEMAN | Sophie TEZENAS DU MONTCEL

¹ARAMIS, Sorbonne Universite, Institut du Cerveau - Paris Brain Institute - ICM, CNRS, Inria, Inserm, AP-HP, Hopital de la Pitie Salpetriere, Paris, France

Correspondence

*Juliette ORTHOLAND

Email: juliette.ortholand@inria.fr,

Adress: 47 Boulevard de l'Hopital, 75013 Paris

Abstract

Non-terminal events can represent a meaningful change in a patient's life. Thus, better understanding and predicting their occurrence can bring valuable information to individuals. In a context where longitudinal markers could inform these events, joint models with competing risks have been developed. Their precision relies on a reference time for which disease onset is often used. Nevertheless, chronic diseases have no clear onset, making it difficult to define a precise reference time.

We propose a Joint cause-specific Spatiotemporal model to overcome this limitation and to capture a shared latent process, a latent age (temporal aspect), associated with the ordering of the longitudinal outcomes (spatial aspect).

First, we validated our model on simulated real-like data. Then, we benchmarked our model with a shared-random-effect joint model on real ALS data using the PRO-ACT dataset. Finally, to show how the model could be used for description tasks, we analysed the impact of sex and onset site on the progression of ALS as well as the initiation of Non-Invasive Ventilation.

The Joint cause-specific spatiotemporal model achieved similar performance to the shared random effect joint model while capturing the latent disease age and the impact of the ordering of longitudinal outcomes on the occurrence of the events with fewer parameters. The application study confirmed existing results for the Longitudinal outcomes and showed how to interpret the model.

The proposed approach by disentangling a temporal and a spatial aspect of the disease opens the perspective to capture meaningful change in future clinical trials.

1 | INTRODUCTION

Detecting clinically meaningful changes for treated patients in clinical trials becomes more and more important (Manta et al., 2020; Weinfurt, 2019). Some clinical scores have been specially created to do so such as Instrumental Activities of Daily Living (Morrow, 1999) or Quality of Life Scale (Burckhardt and Anderson, 2003). Monitoring key events of the diseases, other than death, can also give insight. For instance, the initiation of life-support clinical procedures is an important step in the patient's life and is representative of an advanced stage of the disease. Respiratory failure is the leading cause of death in Amyotrophic Lateral Sclerosis (ALS) and initiation of Non-Invasive Ventilation (NIV), which has been proven to be of effective support (Bourke et al., 2006; Hirose et al., 2018; Kleopa et al., 1999), represent a major step in autonomy loss. The timing anticipation of such non-terminal events remains a challenge for clinicians due to the heterogeneous clinical manifestation of most chronic diseases and modelling could be of great help in such a context.

These events are often censured by death, which violates the non-informative censoring assumption often made in survival analysis (Fleming and Harrington, 2013; D. Jackson et al., 2014). Competing risk models can be used to cope with this issue. Doing so, the quantity of interest is the cumulative incidence function (CIF). Two approaches to model it exist: the cause-specific model, which estimates the hazard by using cause-specific hazard functions to then estimate the CIF (Cheng et al., 1998; Prentice and Gloeckler, 1978) and the Fine and Gray model, which estimates the effect of covariates directly on the CIF by modelling the distribution of hazard functions (Fine and Gray, 1999). The cause-specific model estimates each event separately, and the hazard ratio can thus still be extracted (Andersen et al., 2012; Zhang et al., 2008). Such approach seems more relevant in our context.

Longitudinal outcomes, such as repeated measures of clinical scores or biomarkers, may provide insights into the timing of the initiation of life support intervention and are often jointly available. Different classic models were designed to capture their progression, among which ordinary differential equation models (Lahouel et al., 2023) and Generalised Linear mixed-effects models (GLMM) (McCulloch et al., 2008) are interpretable and describe non-linear progression with individual and population parameters. Nevertheless, in chronic diseases, as described by Young et al., 2024, longitudinal datasets consist in repeated outcomes observed at different time points over a short period of time. The main challenge is thus to realign the individual partial trajectories to reconstruct a long-term disease progression across the disease stages. Data-driven progression models were developed to handle this specificity, alleviating the need for a precise reference time of classic longitudinal models (Schiratti et al., 2015). Among them, the Longitudinal Spatiotemporal model (Schiratti et al., 2015) enables to synchronise patients onto a common disease timeline (temporal aspect) thanks to a latent disease age, while also capturing the remaining variability through parameters that account for the timing and ordering of the outcomes (spatial aspect).

Joint models were developed to model the occurrence of an event jointly with longitudinal data and extended for competing risks. The two main types of joint models are latent class models (Lin et al., 2002; Proust-Lima et al., 2009, 2014) and shared random effect models (Rizopoulos and Ghosh, 2011). Both models rely on GLMM, which restricts their precision to the one of a reference time (Schiratti et al., 2015). First symptoms are often used as reference time to realign trajectories, but in chronic diseases such as ALS, it cannot be accurately estimated (Peter et al., 2017). A joint data-driven progression model was developed, the Joint Temporal model, but only coped with one longitudinal outcome and one event with non-informative censoring (Ortholand et al., 2024).

To bridge this gap, we extended the Joint Temporal model into a Joint cause-specific Spatiotemporal model: the multivariate Longitudinal Spatiotemporal model was associated with a cause-specific Weibull model. We validated it on simulated data and benchmarked it against a shared random effects joint model and the longitudinal Spatiotemporal model on real ALS data. Finally, we show how to use it in a description task, to analyse the

NIV initiation in ALS. We compared the progression speed, the estimated reference time, and spatial variability across sex and onset site subgroups with death and NIV initiation variability.

2 | MODEL SPECIFICATIONS

2.1 | Formalism & Intuitions

2.2 | Notations

In the following, we consider N patients, associated with longitudinal data, y_k , repeated measures of K given outcomes. Each patient i is followed for n_i visits. For each visit j , we denote $t_{i,j,k}$ the age at the visit, and $y_{i,j,k}$ the value of the outcome k for the patient i at this visit j .

For the survival process, following the notation of (Andrinopoulou et al., 2017), we consider L events associated with one timing t_{e_i} that corresponds to the time of the first event observed, or the censoring time. Then, we associated $B_{e_i} = 0$ if the event is censored and $B_{e_i} = l$ if the event l is observed.

2.3 | Joint cause-specific Spatiotemporal model

The Disease Course Map, a non-linear geometric mixed-effect model, was first introduced by Schiratti et al., 2015 and has been then more broadly used for longitudinal process modelling (Koval, 2020; Schiratti, 2017).

2.3.1 | Spatial and temporal random effects

The strength of the Spatiotemporal model is to disentangle temporal from spatial variability.

Temporal variability

First, temporal variability is allowed with variations on individual progression earliness and speed. It is done by mapping the chronological age of a patient t into a latent disease age $\psi_i(t)$, representative of the disease stage of the patient. Using the formalism described before, it can be written as :

$$\psi_i(t) = e^{\xi_i}(t - \tau_i) + t_0 \quad (1)$$

where e^{ξ_i} is the speed factor of patient i , τ_i is its individual estimated reference time and t_0 is the population estimated reference time. $(\tau_i - t_0)$ can thus be seen as an individual time shift compared to the population. Although the reference time is not the time of disease onset, it plays quite the same role: it is a state of the disease on which all the patients are realigned. The main advantage of this formalism is that the individual progressions are realigned on values of the outcomes and not on a reference onset time, as with Generalised Linear Mixed effects models (Schiratti et al., 2015), which might be more robust in our context.

Spatial variability

To capture the disease presentation variability, spatial random effects, named the space-shifts $w_{i,k}$, are defined for each outcome to modify their order of degradation during the disease progression. Nevertheless, for identifiability reasons, the dimension of the space-shift space is reduced with an independent component analysis (ICA) decomposition using $N_s \leq K - 1$ independent sources $(s_i)_{1 \leq i \leq N_s}$, resulting in $w_i = A s_i$, where A is the mixing matrix of the ICA decomposition. However, this definition does not guarantee the orthogonality of the space shift to the speed of progression v_0 (as in the Exp-parallelisation at $\frac{1}{1+g}$ from Riemannian geometry) which gives the identifiability. Thus, the matrix A is defined as a linear combination of vectors of an orthonormal basis, $(B_o)_o$, of the

hyperplane orthogonal to $Span(v_0)$ (dimension $K \times (K - 1)$): each column m of A is thus $A_m = \sum_{o=1}^{K-1} \beta_{o,m} B_o$ with β the matrix of coefficient (dimension $(K - 1) \times N_s$) so that $A = (B\beta)^T$ (Schiratti et al., 2017). These sources are also used to link the survival and the longitudinal process with the creation, for each event l , of a survival shift $u_{i,l} = \sum_{m=1}^{N_s} \zeta_{l,m} s_{i,m}$ with ζ a matrix of hazard ratio coefficients. Note that, to describe individual variability on one longitudinal outcome k or event l , space shift $w_{i,k}$, and survival shifts $u_{i,l}$ are usually easier to interpret compared to sources s_i , as they encapsulate the total effect of the spatial variability on a given outcome.

2.3.2 | Longitudinal submodel

The modelling of the longitudinal process consists of computing the trajectory from the latent disease age defined in section 2.3.1. As we will study clinical scores, with curvilinearity, and potential floor or ceiling effects (Gordon et al., 2010), we modelled logistic function. Thus, we got the average curve for an outcome k at time t :

$$\gamma_{0,k}(t) = \left(1 + g_k \times \exp\left(-\frac{(1+g_k)^2}{g_k}(v_{0,k}(t - t_0))\right) \right)^{-1} \quad (2)$$

where t_0 is the population estimated reference time defined in section 2.3.1, $v_{0,k}$ is the speed of the logistic curves at t_0 and $p_k = \frac{1}{1+g_k}$ is the value of the modelled outcomes at t_0 . We also got the individual curve, adding latent age and spatial variability, for an outcome k (continuous between 0 and 1), an individual i at time t :

$$\gamma_{i,k}(t) = \left(1 + g_k \times \exp\left(-\frac{(1+g_k)^2}{g_k}(v_{0,k}(\psi_i(t) - t_0) + w_{i,k})\right) \right)^{-1} \quad (3)$$

2.3.3 | Survival submodel

We used a cause-specific structure (Cheng et al., 1998; Prentice and Gloeckler, 1978) to handle competing risks. Doing so, for each event l and patient i , we define a hazard $h_{i,l}(t)$, and an associated survival function $S_{i,l}(t)$. The Weibull distribution is used to model the event occurrence from the latent disease age with an additional Cox-proportional hazard impact of the sources on the hazard using the survival shifts $u_i = \zeta s_i$:

$$h_{i,l}(t) = h_{0,i,l}(t) \exp(u_{i,l}) = \frac{\rho_l e^{\zeta_i}}{v_l} \left(\frac{e^{\zeta_i}(t - \tau_l)}{v_l} \right)^{\rho_l - 1} \exp(u_{i,l})$$

where v_l is the scale and ρ_l the shape of the Weibull distribution of the event l . From there, we compute the survival of event l :

$$S_{i,l}(t) = \exp\left(-\int_0^t h_{i,l}(x) dx\right) = \exp\left(-\left(\frac{e^{\zeta_i}(t - \tau_l)}{v_l}\right)^{\rho_l} \exp(u_{i,l})\right)$$

And the Cumulative Incidence Function (CIF) of event l :

$$\begin{aligned} CIF_{i,l}(t) &= \int_0^t h_{i,l}(x) \prod_q^L S_{i,q}(x) dx \\ &= \int_0^t \frac{\rho_l e^{\zeta_i}}{v_l} \left(\frac{e^{\zeta_i}(x - \tau_l)}{v_l} \right)^{\rho_l - 1} \exp(u_{i,l}) \prod_q^L \exp\left(-\left(\frac{e^{\zeta_i}(x - \tau_q)}{v_q}\right)^{\rho_q} \exp(u_{i,q})\right) dx \end{aligned}$$

2.3.4 | Summary

The Joint cause-specific Spatiotemporal model can thus be summarised for a patient i , an outcome k , and an event l by:

$$\begin{cases} \psi_i(t) = e^{\xi_i(t - \tau_i)} + t_0 \\ w_i = A s_i \\ u_i = \zeta s_i \\ \gamma_{i,k}(t) = \left(1 + g_k \times \exp(-v_{0,k} \frac{(g_k+1)^2}{g_k} e^{\xi_i(t - \tau_i)} + w_{i,k})\right)^{-1} \\ S_{i,l}(t) = \exp\left(-\left(\frac{e^{\xi_i(t - \tau_i)}}{v_l}\right)^{\rho_l} \exp(u_{i,l})\right) \end{cases} \quad (4)$$

2.4 | Likelihood of the Joint cause-specific Spatiotemporal model

2.4.1 | Parameters

For estimation purposes, latent parameters (z) are defined in addition to model parameters (θ) and hyperparameters (Π). They can be summarised as follows with the patients indexed by i and outcomes by k , the events by l , the sources by m , and the dimensions of the hyperplane orthogonal to $Span(v_0)$ by o :

- Latent parameters (z):

– Latent fixed effects (z_{fe}): fixed effects sampled

$$\begin{aligned} \tilde{g}_k = \log(g_k) &\sim \mathcal{N}\left(\overline{\tilde{g}_k}, \sigma_{\tilde{g}}^2\right) & \tilde{v}_{0,k} = \log(v_{0,k}) &\sim \mathcal{N}\left(\overline{\tilde{v}_{0,k}}, \sigma_{\tilde{v}_0}^2\right) & \tilde{v}_l = -\log(v_l) &\sim \mathcal{N}\left(\overline{\tilde{v}_l}, \sigma_{\tilde{v}}^2\right) \\ \tilde{\rho}_l = \log(\rho_l) &\sim \mathcal{N}\left(\overline{\tilde{\rho}_l}, \sigma_{\tilde{\rho}}^2\right) & \zeta_{l,m} &\sim \mathcal{N}\left(\overline{\zeta_{l,m}}, \sigma_{\zeta}^2\right) & \beta_{o,m} &\sim \mathcal{N}\left(\overline{\beta_{o,m}}, \sigma_{\beta}^2\right) \end{aligned}$$

– Latent random effects (z_{re}): random effects sampled

$$\xi_i \sim \mathcal{N}\left(\overline{\xi}, \sigma_{\xi}^2\right) \quad \tau_i \sim \mathcal{N}\left(\overline{\tau}, \sigma_{\tau}^2\right) \quad s_{i,m} \sim \mathcal{N}\left(\overline{s}, \sigma_s\right)$$

- Model parameters (θ): fixed effects estimated from log-likelihood maximisation $\theta = \{\overline{\tilde{g}_k}, \overline{\tilde{v}_{0,k}}, \overline{\tilde{v}_l}, \overline{\tilde{\rho}_l}, \overline{\beta_{o,m}}, \overline{\zeta_{l,m}}, \sigma, \sigma_{\xi}, t_0, \sigma_{\tau}\}$
- Hyperparameters (Π): set by the user $\Pi = \{\sigma_{\tilde{g}}, \sigma_{\tilde{v}_0}, \sigma_{\tilde{v}}, \sigma_{\tilde{\rho}}, \sigma_{\beta}, \sigma_{\zeta}, \sigma_s\}$

To ensure identifiability, we set $\overline{\xi} = 0$, $\sigma_s = 1$, $\overline{s} = 0$ and $t_0 = \overline{\tau}$.

2.4.2 | Log-likelihood structure

The likelihood estimated by the model is the following:

$$p(y, T_e, B_e | \theta, \Pi) = \int_z p(y, T_e, B_e, z | \theta, \Pi) dz$$

$p(y, T_e, B_e, z | \theta, \Pi)$ can be divided into four different terms: the longitudinal data attachment, the survival data attachment and two terms for the prior attachment of latent parameters (fixed and random). We end up with the following expression :

$$\begin{aligned} \log p(y, T_e, B_e, z | \theta, \Pi) &= \log p(y | z, \theta, \Pi) + \log p(T_e, B_e | z, \theta, \Pi) \\ &+ \log p(z_{re} | z_{fe}, \theta, \Pi) + \log p(z_{fe} | \theta, \Pi) \end{aligned}$$

The different parts of the log-likelihood are described in appendix A associated with their different assumptions and the full log-likelihood.

2.5 | Estimation of the longitudinal Spatiotemporal model

A first estimation enable to compute fixed and random effects from a training dataset. As there is no analytical solution for maximising the log-likelihood, an Expectation-Maximization algorithm can be used. Nevertheless, the computation of the expectation is also intractable due to the non-linearity of the model. Thus, a Monte-Carlo Markov Chain Stochastic Approximation Expectation-Maximization (MCMC-SAEM) algorithm (Kuhn and Lavielle, 2004) was used with a Robbins-Monro convergence algorithm (Robbins and Monro, 1951) applied on the last iterations to get the mean of the distribution of the model. Note that convergence of the MCMC-SAEM algorithm has been proven for models that lie in the curved exponential family (Kuhn and Lavielle, 2004), a category in which falls the Joint cause-specific Spatiotemporal model. More details are given in appendix B and C.

A second type of estimation enable to compute random effects for a new patient from a test dataset. During this step, we used previously computed fixed effects, thus, only the random effects are estimated. The CIF is needed to compute the predictions and corrected using the survival probability at the last visit used as in (Andrinopoulou et al., 2017). The solver *minimise* from the package Scipy (Virtanen et al., 2020) was used to maximise the log-likelihood. In such context, to speed up the computation the Jacobian of the likelihood regarding the random effects could be useful and is available in appendix D.

An implementation of the Joint cause-specific Spatiotemporal model enabling both estimations is available in the open-source package Leaspy: <https://gitlab.com/icm-institute/aramislab/leaspy>.

2.6 | Reference multivariate and cause-specific models

Different models are used in this article. First, we used one-process-only models. For the survival model, we used a cause-specific Weibull Accelerated Failure Time model to describe the survival process, using the R flexsurv package (C. Jackson, 2016). This model will be referred to as the cause-specific AFT model. For the longitudinal model, we used the Longitudinal Spatiotemporal model described in section 2.3.2 using Leaspy package. This model will be referred to as the Longitudinal model.

Then, we used a joint model with shared random effects for competing risks. We used a logistic longitudinal process, with a cause-specific competing risk model, estimated using the JMbays2 package (Rizopoulos, 2016). This model will be referred to as the cause-specific JMbays2 model. All the model equations are summarised in Table 1.

3 | MATERIAL

3.1 | PRO-ACT data

3.1.1 | Population

We used data from an extraction of 2022 of the Pooled Resource Open-Access ALS Clinical Trials Consortium (PRO-ACT) database, to get estimated real-like values for parameters. This database is a compilation of 23 phase II and III clinical trials along with one observational study. Notably, the database does not include any information that could potentially lead to patient identification, such as the clinical trial, tested drug, study centres, or dates. More detailed information can be found in the paper that introduces the database (Atassi et al., 2014).

We extracted patients from the PRO-ACT database with age at first symptoms, sex, and onset site. To limit left-censored VNI initiation, we selected patients with a Mitos score equal to 0 (Fang et al., 2017). We used this population to extract real-like values for the simulation study and perform the application study. For the benchmark study, we sub-selected this population by keeping only patients with at least three visits to be able to evaluate longitudinal predictions: on the test set, we estimated the random effects of the new patients on their two first visits and made predictions on the remaining.

3.1.2 | Outcome

For the benchmark and the application, we used three subscales of the most widely used functional rating system in patients with ALS, namely the revised version of the ALS functional rating scale revised (ALSFRRs): bulbar scale, fine motor scale, and gross motor scale (Rooney et al., 2017). Indeed, we did not want to use respiratory longitudinal outcomes that risk to capture all the correlations with events.

To test the impact of the number of sources (at a maximum of $K-1$, see section 2.3.1), we wanted to simulate four longitudinal outcomes. We added the ALSFRRs total, which does not make much sense from a clinical point of view, but the idea was only to have credible parameters for the simulation of four outcomes. We normalized the outcomes between 0 (the healthiest value) and +1 (the maximum pathological change). All the scores were normalized using their theoretical maximum and minimum values (Rooney et al., 2017). We reindexed the visits by the time from symptom onset to extract part of the variability and enable a fair comparison with the shared random effect joint model.

We extracted the death, the tracheostomy and NIV initiation age from the PRO-ACT database as described in appendix E.1. As NIV initiation was interval censored, we used the mean of the interval as an approximation, even though this might introduce some biases (Leffondré et al., 2013). Death and tracheostomy were also extracted and associated as in the majority of ALS studies. Note that for simplicity, we will talk about death to encapsulate both, in the following sections. As visits, events were reindexed by the time from symptom onset.

3.2 | Simulated data

Data were simulated under our Joint cause-specific Spatiotemporal model structure. We simulated data thanks to the following procedure:

1. We simulated random effects using $\xi_i \sim \mathcal{N}(0, \sigma_\xi^2)$, $\tau_i \sim \mathcal{N}(t_0, \sigma_\tau^2)$, and N_s sources $s_{i,m} \sim \mathcal{N}(\bar{s}, \sigma_s)$.
2. We modelled age at first visit (baseline) $t_{b,i}$ as $t_{b,i} = \tau_i + \delta_{b,i}$ with $\delta_{b,i} \sim \mathcal{N}(\bar{\delta}_b, \sigma_{\delta_b}^2)$.
3. We set a time of follow-up per patient T_{f_i} , with $T_{f_i} \sim \mathcal{N}(\bar{T}_f, \sigma_{T_f}^2)$ and a time between two visits $\delta_{v_{i,j}} = t_{i,j-1} - t_{i,j}$, with $\delta_{v_i} \sim \mathcal{N}(\bar{\delta}_v, \sigma_{\delta_v}^2)$ to simulate n_i visits until $t_{i,n_i} \leq t_{i,0} + T_{f_i} < t_{i,n_i+1}$.
4. We set the value of the K longitudinal outcomes at each visit using $y_{i,j,k} = \gamma_{i,k}(t_{i,j,k}) + \epsilon_{i,j,k}$ with $\epsilon_{i,j,k} \sim \mathcal{N}(0, \sigma_k^2)$ with Leaspy software.
5. For each patient, we simulated the L event $T_{e_{i,l}}$ using $T_{e_{i,l}} \sim e^{-\xi_i} \mathcal{W}(v_l, \rho_l) + \tau_i$.
6. We kept the first event that occurred as observed and censored the others,
7. We considered that the first event stopped the follow-up and that the follow-up censored the first event. Thus all the visits of each outcome k after the event were censored: $t_{i,j,k} > T_{e_i}$, and events after the last visit were censored: $\max(t_{i,j,k}) < T_{e_i}$.
8. So that all patients had a minimum of two visits, visits were added before the only visit or before the event with a regularity of 1.5 months.

As we studied sub-cores of one score, we considered that all measures were available at a given time. Parameters directly associated with the disease were extracted from data analysis of the PRO-ACT dataset, using the Longitudinal and cause-specific AFT models. Note that some parameter values were adjusted, such as the population estimated reference time, to limit the number of patients with only two visits due to left censoring (Table E1 in appendix). To validate the model and give future users insight on how to select the right number of sources, we simulated four outcomes with two sources, to be able to evaluate the model with 1, 2, and 3 sources. We simulated $M=100$ datasets with $N=300$ patients. The parameters used for the simulation study are summarised in Table E1 in the appendix.

3.3 | Characteristics of the datasets

Out of the 8,571 patients from the PRO-ACT database, we subselected 6,034 patients with sex and first symptoms (spinal or bulbar onset) provided. Out of them, 2,219 had their first visit with a Mitos score equal to 0. Then 42 patients were dropped for the Analysis dataset due to left censored VNI. For the Benchmark dataset, we also dropped patients with less than 3 visits and ended up with 1,919 patients. Characteristics of the Analysis and the Benchmark dataset were close despite the subselection of patients (Table 2). NIV initiation was interval censored between two visits, with a mean interval of 1.9 (1.4) months.

Simulated scenarios had fewer patients and visits than the PRO-ACT datasets but the rest of the different characteristics were relatively close (Table 2).

4 | SIMULATION STUDY

The objective of this section was to validate the Joint cause-specific Spatiotemporal model by assessing fixed and random effects estimation on simulated data. Note that including section 3, we used the ADEMP method for the simulation study (Morris et al., 2019).

4.1 | Method

4.1.1 | Estimands

For each experiment, we initialised the Joint Temporal model with the Longitudinal model trained for 2,000 iterations and a survival Weibull model. Then, we ran the Joint Temporal model with 50,000 iterations (on average two hours) with the last 10,000 of the Robbins-Monro convergence phase (Robbins and Monro, 1951) to extract the mean of the posterior. The value of the hyperparameter number of sources which corresponds to the number of dimensions allowed for the ordering of the longitudinal outcomes (spatial aspect) was selected using BIC adapted for mixed effect models (Delattre et al., 2014). Experiments that validate this method can be found in appendix H.

On both simulated datasets, we validated the estimation of the model parameters $\theta = \{\sigma_{\xi}, \sigma_{\tau}, t_0, \bar{g}, \bar{v}_0, \bar{v}, \bar{\rho}, \sigma\}$ extracted by the Robbins-Monro convergence phase. As we use a Gaussian approximation for the noise, we estimated σ using the noisy simulation and the expected exact curve simulated from the random effect. No Robbins-Monro convergence phase was applied to the random effects (τ_i, ξ_i, w_i) , we thus extracted the mean of the last 100 iterations for each individual.

4.1.2 | Performance metrics

To assess the estimation performances of the estimated model parameters ($\hat{\theta}$) over the M datasets simulated for the scenario, we reported:

- the Relative Bias: $RB(\hat{\theta}) = \frac{1}{M} \sum_{m=1}^M \frac{\hat{\theta}^{(m)} - \theta}{\theta} \times 100$
- Relative Root Mean Square Errors: $RRMSE(\hat{\theta}) = \sqrt{\frac{1}{M} \sum_{m=1}^M \left(\frac{\hat{\theta}^{(m)} - \theta}{\theta} \times 100 \right)^2}$
- Relative Estimation Errors: $REE^{(m)} = \frac{\hat{\theta}^{(m)} - \theta}{\theta} \times 100$

To assess the Standard Error of the estimated model parameters ($\hat{\theta}$), we reported:

- the coverage rates (CR): defined as the proportion of datasets for which θ belonged to $[\hat{\theta} - 1.96SE(\hat{\theta}), \hat{\theta} + 1.96SE(\hat{\theta})]$ with their 95% confidence intervals (CI) computed using the exact Clopper Pearson method.

The estimation of the random effects (τ_i, ξ_i, w_i) was assessed using the intraclass correlation between the mean of each individual and the true value that enabled the simulation.

4.2 | Results

For fixed effects, the relative bias (RB) was smaller than 20% in absolute and the Relative Root Mean Square Errors (RRMSE) was below 25% (Table 3). Coverage rates were correct with respect to the difficulty of the scenario simulated with 8 out of 19 containing 95 and 18 out of 19 containing 80 (Table 3). The relative estimation errors extracted from the 100 datasets simulated were quite centred on 0 (Figure F2).

Random effects had an intraclass correlation above 0.84 except for survival shifts for which the intraclass correlation was of 0.479 (0.416) for the one associated with NIV and of 0.147 (0.445) for the one associated with death (Table F2 in appendix). This is due to the small number of observed events.

5 | BENCHMARK

The objective of this section was to evaluate if our model could improve prediction compared to the cause-specific JMBayes2 and the Longitudinal model.

5.1 | Method

We made a 10-fold cross-validation (train 90% - test 10%) on the Benchmark dataset. For each Joint cause-specific Spatiotemporal model, we first trained the Longitudinal model for 2,000 iterations. Then, we ran the Joint cause-specific Spatiotemporal model for 70,000 iterations (on average 7 hours) using the values of the Longitudinal model as initialisation (with a Robbins-Monro convergence phase on the 10,000 last iterations (Robbins and Monroe, 1951)). The cause-specific JMBayes2 model ran for 25,000 iterations (on average 3 hours and a half). The Longitudinal model was also run for 70,000 iterations (with a Robbins-Monro convergence phase on the 10,000 last iterations (Robbins and Monroe, 1951)).

We compared the models using prediction of both longitudinal and survival outcomes: we estimated the random effects of the new patients on the two first visits of the patients from the tests set and made predictions on the remaining. The goodness of longitudinal predictions was assessed using absolute errors for each of the three longitudinal outcomes.

We assessed the goodness of survival predictions in ordering events using the C-index at 1 and 1.5 years and the

mean cumulative dynamic AUC at 1 and 1.5 years (which is known to be more robust (Blanche et al., 2019)). We used the Integrated Brier Score (IBS) to evaluate the precision of predictions of survival predictions. All the survival metrics were computed using the Python package `sksurv` (Pölsterl, 2020). The predictions were compared using a Wilcoxon signed-rank test with a Bonferroni correction.

5.2 | Results

12,197 longitudinal predictions were made at 0.55 (0.47) years from the last visit. The Longitudinal model was significantly better than the Joint cause-specific Spatiotemporal model for all the different outcomes, even though the difference was small: the larger being for gross motor scale with 1.424 (1.331) against 1.414 (1.335) (p-value = $6.5e-30$) (Table 4). The cause-specific JMBayes2 model got a significantly lower absolute bias with a small magnitude for two outcomes compared to the Joint cause-specific Spatiotemporal model: for bulbar scale (1.166 (1.233) against 1.187 (1.312) (p-value: $3.4e-02$)) and gross motor scale (1.365 (1.288) against 1.424 (1.331) (p-value: $3.4e-02$)) (Table 4).

The Joint cause-specific Spatiotemporal model got systematically better AUC and C-index compared to the cause-specific JMBayes2 model, but none was significant (NIV AUC 0.642 (0.085) (p-value: $1.0e+00$) against 0.633 (0.091) and death AUC 0.719 (0.101) against 0.695 (0.107) (p-value: $1.7e-01$)) (Table 5). For the IBS, the cause-specific JMBayes2 model got significantly better results with small magnitude for the IBS for both NIV initiation (0.124 (0.015) against 0.131 (0.013) (p-value: $7.8e-03$)) and death (0.138 (0.021) against 0.142 (0.02) (p-value: $1.3e-06$)) (Table 5).

6 | APPLICATION

The objective of this section was to show how the Joint cause-specific model can be used to analyse NIV initiation.

6.1 | Method

We chose the number of sources using the extended BIC (Delattre et al., 2014) as validated in appendix H. Prediction performances described above are in favour of a shared latent age. Nevertheless, we still wanted to assess this hypothesis. Following a study available in appendix I, we especially checked that the shape parameter of the Weibull distribution described the same hazard function. Indeed, depending on the value of the shape parameter of the Weibull distribution (ρ) the hazard function $h(t)$ has different progressions ($\rho < 1$: the hazard function decreases over time, $\rho = 1$: the hazard function is constant, $\rho > 1$: the hazard function increases with time) (Jiang and Murthy, 2011).

We ran one model on the Analysis PRO-ACT dataset for 50,000 iterations (with a Robbins-Monro convergence phase on the 10,000 last iterations (Robbins and Monro, 1951)). We extracted from the individual posteriors the mean of the random effects from the last 100 iterations (between 40,000 and 50,000 before the Robin-Monro scheme (Robbins and Monro, 1951)).

Then, to better characterize the heterogeneity associated with sex (man/woman) and onset site (spinal/bulbar), we studied the distribution of random effects according to four subgroups using ANOVA with Bonferroni correction.

6.2 | Results

The number of sources must be inferior or equal to the number of outcomes studied minus one, thus in our case, we tested one and two sources. We computed the extended BIC for the model with one (-41,548) and two sources (-56,107) and chose to use two sources. The parameters of the Weibull distribution estimated were close to the one of the competing risk analyses alone and described the same hazard progression (Table G3 in appendix) which enabled us to validate the hypothesis of the shared latent age.

Here we mainly focus on the random effects as their structure is the main novelty of the Joint cause-specific model, but all the fixed effects of the model are available in Table G4 in the appendix.

Temporal variability

The estimated reference time was not significantly different between the four studied groups (Figure 1 A).

We did not find any significant interaction between the onset site and sex for the speed factor of progression (p-value = 1.) (Figure 1 B). However, patients with bulbar onset were found to progress 1.47 times faster (95% CI = [1.37, 1.58]) than patients with spinal onset independently of sex.

Individual spatial variability

Sources characterise the dimensions of spatial variability, i.e. the order of evolution of longitudinal outcomes and their impact on events. Nevertheless, to describe individual variability on one longitudinal outcome k or event l , space shift ($w_{i,k} = A_k s_i$) and survival shifts ($u_{i,l} = \zeta_l s_i$) are usually easier to interpret compared to sources s_i , as they encapsulate the total effect of the spatial variability (see section 2.3.1). Note that survival shifts have a proportional impact on the hazard and their interpretation is close to the one of the hazard ratio and will be referred to as the Proportional effect of survival shifts on the Hazard (PH). The space shifts were corrected by the speed (v_0) to be on a time unit.

As we are more interested in the method to analyse the results rather than the results themselves, we only analyse one space shift and one survival shift here, but the rest of the interpretation can be found in appendix G.1. Using the space shift associated with the bulbar scale $w_i v_0^{-1}$, we did not observe any interaction between sex and onset site for ALSFRSr bulbar scale (p-value = 0.15), once corrected for the estimated reference timing and speed of progression (Figure 1 C). ALSFRSr bulbar scale deteriorated 28.6 months later (95% CI = [27.4, 29.9]) for patients with spinal onset compared to bulbar onset, independently of the sex.

Using the survival shift associated with the initiation of NIV u_i , after correction for speed and onset, women had a significantly higher risk of NIV initiation compared to men (PH: 1.09 [1.08, 1.11]) (Figure 1 D).

7 | DISCUSSION

We designed the first data-driven multivariate joint cause-specific model. To do so, we used the Longitudinal Spatiotemporal model as longitudinal submodel. The proposed Joint cause-specific Spatiotemporal model realigns both survival and longitudinal observations on a latent disease age (temporal aspect). In addition, it captures the impact of the order of the longitudinal outcome on the survival processes (spatial aspect). This enabled us to overcome the limitation of the joint shared random effects that model the impact of the longitudinal outcomes on survival.

After validating it on simulation data close to real-life data we have benchmarked it in prediction against a joint shared random effect model using JMBayes2 package (Rizopoulos, 2016). The joint shared random effect model got better results for all the longitudinal outcomes. This might be the drawback of one shared individual speed (ξ_i) of the Spatiotemporal model. Nevertheless, this shared individual speed should facilitate application

to a higher number of longitudinal outcomes, which is currently a limitation of the joint shared random effect model (Devaux et al., 2023; Hickey et al., 2016). Compared to the Joint cause-specific Spatiotemporal model, the Longitudinal Spatiotemporal model got significantly better results. This could be because the longitudinal model is less constrained.

For survival metrics, even though the Joint cause-specific Spatiotemporal model got systematically better event ordering metrics (C-index and AUC) compared to the joint shared random effect model, none was significant. This might point out the interest of the latent age to capture individual variability. The joint shared random effect model got better results for the event distance metric (IBS). The survival function of the joint shared random effect model may exhibit this difference due to its enhanced flexibility, utilizing splines instead of a Weibull function.

We demonstrate how the different random effects can be interpreted in order to analyse the progression of ALS. We confirmed some known results on the longitudinal data (Grassano et al., 2024; Ortholand et al., 2024). More observed events as well as analysis including covariates, left and interval censored events would be necessary to replicate results on NIV (Dibling et al., 2024; Grassano et al., 2024).

The designed model showed great potential to model a shared disease speed among both longitudinal and survival processes, which offer a new modelling perspective. Nevertheless, its structure makes it harder to model complex associations, such as the impact of the integral of some outcomes, which is possible with JMBayes2. Covariates were also not included in the model, but recent work (Fournier and Durrleman, 2023) paves the way for their integration. Finally, improvements in dealing with survival data could be done by handling interval and left censored events to reduce potential introduced biases (Leffondré et al., 2013) as well as more flexible hazard function with splines for example.

We have encompassed the different aspects of the use of a model in terms of the description and prediction of real data. We have provided an open-source tool for its future use (<https://gitlab.com/icm-institute/aramislab/leaspy>). Nevertheless, more simulation work would be needed to fully assess the performances and the limits of the model, but this was out of the scope of this article (Heinze et al., 2024). In that direction, a benchmark in the context of higher dimensions could be of interest (Devaux et al., 2023; Hickey et al., 2016; Nguyen et al., 2023).

In conclusion, the proposed multivariate joint cause-specific model with latent disease age enabled us to offer a new modelling framework and alleviate the need for a precise reference time. This model opens up the perspective to design predictive and personalized therapeutic strategies.

References

- Andersen, P. K., Geskus, R. B., de Witte, T., & Putter, H. (2012). Competing risks in epidemiology: Possibilities and pitfalls. *International Journal of Epidemiology*, 41(3), 861–870. <https://doi.org/10.1093/ije/dyr213>
- Andrinopoulou, E.-R., Rizopoulos, D., Takkenberg, J. J., & Lesaffre, E. (2017). Combined dynamic predictions using joint models of two longitudinal outcomes and competing risk data. *Statistical Methods in Medical Research*, 26(4), 1787–1801. <https://doi.org/10.1177/0962280215588340>
- Atassi, N., Berry, J., Shui, A., Zach, N., Sherman, A., Sinani, E., Walker, J., Katsovskiy, I., Schoenfeld, D., Cudkovicz, M., & Leitner, M. (2014). The PRO-ACT database: Design, initial analyses, and predictive features. *Neurology*, 83(19), 1719–1725. <https://doi.org/10.1212/WNL.0000000000000951>
- Blanche, P., Kattan, M. W., & Gerds, T. A. (2019). The c-index is not proper for the evaluation of t-year predicted risks. *Biostatistics*, 20(2), 347–357. <https://doi.org/10.1093/biostatistics/kxy006>
- Bourke, S. C., Tomlinson, M., Williams, T. L., Bullock, R. E., Shaw, P. J., & Gibson, G. J. (2006). Effects of non-invasive ventilation on survival and quality of life in patients with amyotrophic lateral sclerosis: A

- randomised controlled trial [Publisher: Elsevier]. *The Lancet Neurology*, 5(2), 140–147. [https://doi.org/10.1016/S1474-4422\(05\)70326-4](https://doi.org/10.1016/S1474-4422(05)70326-4)
- Burckhardt, C. S., & Anderson, K. L. (2003). The quality of life scale (qols): Reliability, validity, and utilization. *Health and Quality of Life Outcomes*, 1, 60. <https://doi.org/10.1186/1477-7525-1-60>
- Cheng, S. C., Fine, J. P., & Wei, L. J. (1998). Prediction of cumulative incidence function under the proportional hazards model. *Biometrics*, 54(1), 219–228.
- Delattre, M., Lavielle, M., & Poursat, M.-A. (2014). A note on BIC in mixed-effects models. *Electronic Journal of Statistics*, 8(1), 456–475. <https://doi.org/10.1214/14-EJS890>
- Devaux, A., Helmer, C., Genuer, R., & Proust-Lima, C. (2023, February). *Random survival forests with multivariate longitudinal endogenous covariates* [Doctoral dissertation] [arXiv:2208.05801 [stat]]. arXiv. <https://doi.org/10.48550/arXiv.2208.05801>
- Dibling, M., Ortholand, J., Salachas, F., Hesters, A., & Montcel, T. D. (2024). Care pathway heterogeneity in Amyotrophic Lateral Sclerosis: Effects of gender, age and onset. [Manuscript submitted for publication].
- Fang, T., Al Khleifat, A., Stahl, D. R., Lazo La Torre, C., Murphy, C., Young, C., Shaw, P. J., Leigh, P. N., & Al-Chalabi, A. (2017). Comparison of the King's and MiToS staging systems for ALS. *Amyotrophic Lateral Sclerosis & Frontotemporal Degeneration*, 18(3-4), 227–232. <https://doi.org/10.1080/21678421.2016.1265565>
- Fine, J. P., & Gray, R. J. (1999). A Proportional Hazards Model for the Subdistribution of a Competing Risk [Publisher: [American Statistical Association, Taylor & Francis, Ltd.]]. *Journal of the American Statistical Association*, 94(446), 496–509. <https://doi.org/10.2307/2670170>
- Fleming, T. R., & Harrington, D. P. (2013, August). *Counting Processes and Survival Analysis* [Google-Books-ID: vam6EAAAQBAJ]. John Wiley & Sons.
- Fournier, N., & Durrleman, S. (2023). A Multimodal Disease Progression Model for Genetic Associations with Disease Dynamics. In H. Greenspan, A. Madabhushi, P. Mousavi, S. Salcudean, J. Duncan, T. Syeda-Mahmood, & R. Taylor (Eds.), *Medical Image Computing and Computer Assisted Intervention – MICCAI 2023* (pp. 601–610). Springer Nature Switzerland. https://doi.org/10.1007/978-3-031-43904-9_58
- Gordon, P. H., Cheng, B., Salachas, F., Pradat, P.-F., Bruneteau, G., Corcia, P., Lacomblez, L., & Meininger, V. (2010). Progression in ALS is not linear but is curvilinear. *Journal of Neurology*, 257(10), 1713–1717. <https://doi.org/10.1007/s00415-010-5609-1>
- Grassano, M., Moglia, C., Palumbo, F., Koumantakis, E., Cugnasco, P., Callegaro, S., Canosa, A., Manera, U., Vasta, R., De Mattei, F., Matteoni, E., Fuda, G., Salamone, P., Marchese, G., Casale, F., De Marchi, F., Mazzini, L., Mora, G., Calvo, A., & Chiò, A. (2024). Sex Differences in Amyotrophic Lateral Sclerosis Survival and Progression: A Multidimensional Analysis [eprint: <https://onlinelibrary.wiley.com/doi/pdf/10.1002/ana.26933>]. *Annals of Neurology*, n/a(n/a). <https://doi.org/10.1002/ana.26933>
- Heinze, G., Boulesteix, A.-L., Kammer, M., Morris, T. P., White, I. R., & Initiative, t. S. P. o. t. S. (2024). Phases of methodological research in biostatistics—Building the evidence base for new methods. *Biometrical Journal*, 66(1), 2200222. <https://doi.org/10.1002/bimj.202200222>
- Hickey, G. L., Philipson, P., Jorgensen, A., & Kolamunnage-Dona, R. (2016). Joint modelling of time-to-event and multivariate longitudinal outcomes: Recent developments and issues. *BMC Medical Research Methodology*, 16(1), 117. <https://doi.org/10.1186/s12874-016-0212-5>
- Hirose, T., Kimura, F., Tani, H., Ota, S., Tsukahara, A., Sano, E., Shigeikiyo, T., Nakamura, Y., Kakiuchi, K., Motoki, M., Unoda, K., Ishida, S., Nakajima, H., & Arawaka, S. (2018). Clinical characteristics of long-term survival with noninvasive ventilation and factors affecting the transition to invasive ventilation in amyotrophic lateral sclerosis. *Muscle & Nerve*, 58(6), 770–776. <https://doi.org/10.1002/mus.26149>

- Jackson, C. (2016). **flexsurv** : A Platform for Parametric Survival Modeling in R. *Journal of Statistical Software*, 70(8). <https://doi.org/10.18637/jss.v070.i08>
- Jackson, D., White, I. R., Seaman, S., Evans, H., Baisley, K., & Carpenter, J. (2014). Relaxing the independent censoring assumption in the Cox proportional hazards model using multiple imputation. *Statistics in Medicine*, 33(27), 4681–4694. <https://doi.org/10.1002/sim.6274>
- Jiang, R., & Murthy, D. N. P. (2011). A study of Weibull shape parameter: Properties and significance. *Reliability Engineering & System Safety*, 96(12), 1619–1626. <https://doi.org/10.1016/j.res.2011.09.003>
- Kleopa, K. A., Sherman, M., Neal, B., Romano, G. J., & Heiman-Patterson, T. (1999). Bipap improves survival and rate of pulmonary function decline in patients with ALS [Publisher: Elsevier]. *Journal of the Neurological Sciences*, 164(1), 82–88. [https://doi.org/10.1016/S0022-510X\(99\)00045-3](https://doi.org/10.1016/S0022-510X(99)00045-3)
- Koval, I. (2020). Learning Multimodal Digital Models of Disease Progression from Longitudinal Data: Methods & Algorithms for the Description, Prediction and Simulation of Alzheimer’s Disease Progression, 181.
- Kuhn, E., & Lavielle, M. (2004). Coupling a stochastic approximation version of EM with an MCMC procedure [Publisher: EDP Sciences]. *ESAIM: Probability and Statistics*, 8, 115–131. <https://doi.org/10.1051/ps:2004007>
- Lahouel, K., Wells, M., Rielly, V., Lew, E., Lovitz, D., & Jedynek, B. M. (2023, November). Learning nonparametric ordinary differential equations from noisy data [arXiv:2206.15215 [cs, stat]]. <https://doi.org/10.48550/arXiv.2206.15215>
- Lavalley-Morelle, A., Mentré, F., Comets, E., & Mullaert, J. (2024). Extending the code in the open-source saemix package to fit joint models of longitudinal and time-to-event data. *Computer Methods and Programs in Biomedicine*, 247, 108095. <https://doi.org/10.1016/j.cmpb.2024.108095>
- Leffondré, K., Touraine, C., Helmer, C., & Joly, P. (2013). Interval-censored time-to-event and competing risk with death: Is the illness-death model more accurate than the Cox model? *International Journal of Epidemiology*, 42(4), 1177–1186. <https://doi.org/10.1093/ije/dyt126>
- Lin, H., Turnbull, B. W., McCulloch, C. E., & Slate, E. H. (2002). Latent Class Models for Joint Analysis of Longitudinal Biomarker and Event Process Data: Application to Longitudinal Prostate-Specific Antigen Readings and Prostate Cancer. *Journal of the American Statistical Association*, 97(457), 53–65. <https://doi.org/10.1198/016214502753479220>
- Manta, C., Patrick-Lake, B., & Goldsack, J. C. (2020). Digital measures that matter to patients: A framework to guide the selection and development of digital measures of health. *Digital Biomarkers*, 4(3), 69–77. <https://doi.org/10.1159/000509725>
- McCulloch, C. E., Searle, S. R., & Neuhaus, J. M. (2008, June). *Generalized, Linear, and Mixed Models* [Google-Books-ID: iDg0QwAACAAJ]. Wiley.
- Morris, T. P., White, I. R., & Crowther, M. J. (2019). Using simulation studies to evaluate statistical methods. *Statistics in Medicine*, 38(11), 2074–2102. <https://doi.org/10.1002/sim.8086>
- Morrow, S. (1999). Instrumental activities of daily living scale. *AJN The American Journal of Nursing*, 99(1), 24CC.
- Mozumder, S. I., Rutherford, M. J., & Lambert, P. C. (2018). Direct likelihood inference on the cause-specific cumulative incidence function: A flexible parametric regression modelling approach. *Statistics in medicine*, 37(1), 82–97. <https://doi.org/10.1002/sim.7498>
- Nesterov, Y. (2018). *Lectures on Convex Optimization* (Vol. 137). Springer International Publishing. <https://doi.org/10.1007/978-3-319-91578-4>
- Nguyen, V. T., Fermanian, A., Guilloux, A., Barbieri, A., Zohar, S., Jannot, A.-S., & Bussy, S. *FLASH: A Fast joint model for Longitudinal And Survival data in High dimension*. en. 2023, September. <https://doi.org/arXiv:2309.03714>[stat] arXiv: 2309.03714 [stat.ME].

- Ortholand, J., Gensollen, N., Durrleman, S., & Montcel, S. T. d. (2024). Joint model with latent disease age: Overcoming the need for reference time [arXiv:2401.17249 [stat]]. [Manuscript submitted for publication]. Retrieved May 3, 2024, from <http://arxiv.org/abs/2401.17249>
- Peter, R. S., Rosenbohm, A., Dupuis, L., Brehme, T., Kassubek, J., Rothenbacher, D., Nagel, G., & Ludolph, A. C. (2017). Life course body mass index and risk and prognosis of amyotrophic lateral sclerosis: Results from the ALS registry Swabia. *European Journal of Epidemiology*, *32*(10), 901–908. <https://doi.org/10.1007/s10654-017-0318-z>
- Pölsterl, S. (2020). Scikit-survival: A library for time-to-event analysis built on top of scikit-learn. *Journal of Machine Learning Research*, *21*(212), 1–6. <http://jmlr.org/papers/v21/20-729.html>
- Prentice, R. L., & Gloeckler, L. A. (1978). Regression Analysis of Grouped Survival Data with Application to Breast Cancer Data. *Biometrics*, *34*(1), 57. <https://doi.org/10.2307/2529588>
- Proust-Lima, C., Joly, P., Dartigues, J.-F., & Jacqmin-Gadda, H. (2009). Joint modelling of multivariate longitudinal outcomes and a time-to-event: A nonlinear latent class approach. *Computational Statistics & Data Analysis*, *53*(4), 1142–1154. <https://doi.org/10.1016/j.csda.2008.10.017>
- Proust-Lima, C., Séne, M., Taylor, J. M., & Jacqmin-Gadda, H. (2014). Joint latent class models for longitudinal and time-to-event data: A review [Publisher: SAGE Publications Ltd STM]. *Statistical Methods in Medical Research*, *23*(1), 74–90. <https://doi.org/10.1177/0962280212445839>
- Rizopoulos, D. (2016). The R Package **JMbayes** for Fitting Joint Models for Longitudinal and Time-to-Event Data Using MCMC. *Journal of Statistical Software*, *72*(7). <https://doi.org/10.18637/jss.v072.i07>
- Rizopoulos, D., & Ghosh, P. (2011). A Bayesian semiparametric multivariate joint model for multiple longitudinal outcomes and a time-to-event [_eprint: <https://onlinelibrary.wiley.com/doi/pdf/10.1002/sim.4205>]. *Statistics in Medicine*, *30*(12), 1366–1380. <https://doi.org/10.1002/sim.4205>
- Robbins, H., & Monro, S. (1951). A Stochastic Approximation Method [Publisher: Institute of Mathematical Statistics]. *The Annals of Mathematical Statistics*, *22*(3), 400–407. <https://doi.org/10.1214/aoms/1177729586>
- Rooney, J., Burke, T., Vajda, A., Heverin, M., & Hardiman, O. (2017). What does the ALSFRS-R really measure? A longitudinal and survival analysis of functional dimension subscores in amyotrophic lateral sclerosis. *Journal of Neurology, Neurosurgery, and Psychiatry*, *88*(5), 381–385. <https://doi.org/10.1136/jnnp-2016-314661>
- Schiratti, J.-B., Allasonnière, S., Routier, A., Colliot, O., & Durrleman, S. (2015). A Mixed-Effects Model with Time Reparametrization for Longitudinal Univariate Manifold-Valued Data. In S. Ourselin, D. C. Alexander, C.-F. Westin, & M. J. Cardoso (Eds.), *Information Processing in Medical Imaging* (pp. 564–575). Springer International Publishing. https://doi.org/10.1007/978-3-319-19992-4_44
- Schiratti, J.-B. (2017). Methods and algorithms to learn spatio-temporal changes from longitudinal manifold-valued observations, 200.
- Schiratti, J.-B., Allasonnière, S., Colliot, O., & Durrleman, S. (2017). A Bayesian Mixed-Effects Model to Learn Trajectories of Changes from Repeated Manifold-Valued Observations, 33.
- Virtanen, P., Gommers, R., Oliphant, T. E., Haberland, M., Reddy, T., Cournapeau, D., Burovski, E., Peterson, P., Weckesser, W., Bright, J., van der Walt, S. J., Brett, M., Wilson, J., Millman, K. J., Mayorov, N., Nelson, A. R. J., Jones, E., Kern, R., Larson, E., ... SciPy 1.0 Contributors. (2020). SciPy 1.0: Fundamental Algorithms for Scientific Computing in Python. *Nature Methods*, *17*, 261–272. <https://doi.org/10.1038/s41592-019-0686-2>
- Weinfurt, K. P. (2019). Clarifying the meaning of clinically meaningful benefit in clinical research: Noticeable change vs valuable change. *JAMA*, *322*(24), 2381–2382. <https://doi.org/10.1001/jama.2019.18496>

- Young, A. L., Oxtoby, N. P., Garbarino, S., Fox, N. C., Barkhof, F., Schott, J. M., & Alexander, D. C. (2024). Data-driven modelling of neurodegenerative disease progression: Thinking outside the black box [Publisher: Nature Publishing Group]. *Nature Reviews Neuroscience*, 1–20. <https://doi.org/10.1038/s41583-023-00779-6>
- Zhang, M.-J., Zhang, X., & Scheike, T. H. (2008). Modeling cumulative incidence function for competing risks data. *Expert review of clinical pharmacology*, 1(3), 391–400. <https://doi.org/10.1586/17512433.1.3.391>

Table 1 Specification of used models for multivariate longitudinal outcomes and competing risks

Legend: Longitudinal: Longitudinal Spatiotemporal model, Cause-specific AFT: Cause-specific Weibull Accelerated Failure Time model, Joint Spatiotemporal: the Joint cause-specific Spatiotemporal model, Cause-specific-JMbayes2: joint model with shared random effects and cause-specific survival model. spl(t): spline function. L events indexed by l and K longitudinal outcomes indexed by k. For space reasons, the CIF is not integrated into the table, but all the model followed a cause-specific structure described in (Zhang et al., 2008) and in section 2.3.3

Model	Inputs	Effects		Random effects structure $\psi_i(t)$	Link functions	
		Fixed	Random		Longitudinal $\gamma_{i,k}(t)$	$S_{i,l}(t)$
Longitudinal	t	g, ν_0, t_0	ξ_i, τ_i, w_i	$e^{\xi_i(t - \tau_i) + t_0}$	$\left(1 + g_k \times \exp(-\nu_{0,k} \frac{(g_k+1)^2}{g_k} (\psi_i(t) - t_0) + w_{i,k})\right)^{-1}$	-
Cause-specific AFT	t	ν_0, ρ_0	-	-	-	$\exp\left(-\left(\frac{t}{\nu_i}\right)^{\rho_i}\right)$
Joint Spatiotemporal	t	g, ν_0, t_0, ρ, ν	ξ_i, τ_i, w_i, u_i	$e^{\xi_i(t - \tau_i) + t_0}$	$\left(1 + g_k \times \exp(-\nu_{0,k} \frac{(g_k+1)^2}{g_k} (\psi_i(t) - t_0) + w_{i,k})\right)^{-1}$	$\exp\left(-\left(\frac{\psi_i(t)}{\nu_i}\right)^{\rho_i} \exp(u_{i,l})\right)$
Cause-specific-JMbayes2	t	$\beta_0, \beta_1, g_k, \alpha, spl(t)$	$b_{i,0}, b_{i,1}$	$(\beta_0 + b_{i,0}) + (\beta_1 + b_{i,1})t$	$(1 + g_k \times \exp(\psi_i(t)))^{-1}$	$\exp\left(-\int_0^t \exp(spl_l(u) + \sum_k \alpha_k \gamma_{i,k}(u)) du\right)$

Table 2 Characteristics of the PRO-ACT and real-like simulated dataset

Legend: Results are presented with mean (SD) [class%]. There were no missing values in the dataset due to patient selection.

Analysis: extraction from the PRO-ACT database used for the application and the estimation of parameters used for simulation, Benchmark: extraction from PRO-ACT database used to benchmark the models, patients have at least 3 visits, Real-like: first real-like dataset simulated over the 100.

Type	Characteristics	Real PRO-ACT data		Simulated data
		Analysis	Benchmark	Real-like
Number	patients	2,177	1,919	300
	visits	16,400	16,036	2,065
	patient-years	1,661	1,650	287
	visits per patients	7.5 (4.5)	8.4 (4.1)	6.9 (3.2)
Time	follow-up (years)	0.8 (0.5)	0.9 (0.5)	1.0 (0.5)
	between visits (months)	1.4 (0.7)	1.4 (0.7)	2.0 (0.7)
Gender	(Male)	1,364 [62.7 %]	1197 [62.4 %]	-
Symptom onset	(Spinal)	1,666 [76.5 %]	1465 [76.3 %]	-
Age at first symptoms		54.1 (11.3)	54.0 (11.4)	-
Observed events (%)	VNI	570 [26.2%]	477 [24.9%]	72 [24.0 %]
	Death	245 [11.3%]	216 [11.3%]	28 [9.3 %]
ALSFRS _r (baseline)	total	39.4 (4.1)	39.6 (4.1)	40.6 (3.8)
	bulbar	10.3 (2.0)	10.3 (2.0)	10.6 (1.9)
	fine motor	9.1 (2.0)	9.1 (2.0)	9.7 (2.0)
	gross motor	8.5 (2.4)	8.6 (2.5)	9.1 (2.4)

Table 3 Validation metrics for the fixed effects of the Joint cause-specific Spatiotemporal model on the Real-like simulated dataset

Legend: Simulated: the value of the parameter used for simulation, RB(%): the relative bias, RRMSE (%): the relative root mean square error, CR(%): the 95 % coverage intervals. $\bar{\xi}, \bar{s}, \sigma_s$ parameters are not present as they are fixed by the model ($\bar{\xi} = 0, \bar{s} = 0, \sigma_s = 1$) and $t_0 = \bar{\tau}$

Parameters name		Simulated	RB (%)	RRMSE (%)	CR (%)	
Distribution of random effects	Estimated reference time (mean)	t_0	5.000	0.10	2.23	94.0 [87.4, 97.8]
	Estimated reference time (std)	σ_τ	1.000	-1.47	4.40	96.0 [90.1, 98.9]
	Individual log-speed factor (std)	σ_ξ	0.790	13.21	14.85	52.0 [41.8, 62.1]
Longitudinal fixed effects	Curve values at $t_0: \frac{1}{1+g_k} (g_k)$	g_0	13.958	-5.35	9.28	90.0 [82.4, 95.1]
		g_1	5.316	-8.08	11.27	81.0 [71.9, 88.2]
		g_2	3.993	-7.74	10.87	81.0 [71.9, 88.2]
		g_3	5.704	-5.93	7.71	74.0 [64.3, 82.3]
	Speed of the logistic curves ($v_{0,k}$)	$v_{0,0}$	0.069	-7.04	10.87	84.0 [75.3, 90.6]
		$v_{0,1}$	0.188	-7.43	10.64	84.0 [75.3, 90.6]
		$v_{0,2}$	0.198	-8.89	11.27	78.0 [68.6, 85.7]
		$v_{0,3}$	0.112	-9.34	11.21	73.0 [63.2, 81.4]
	Estimated noises (σ_k)	σ_0	0.066	-3.22	4.12	78.0 [68.6, 85.7]
		σ_1	0.102	-1.08	2.44	92.0 [84.8, 96.5]
		σ_2	0.102	-0.82	2.24	94.0 [87.4, 97.8]
		σ_3	0.046	0.17	2.14	95.0 [88.7, 98.4]
	Survival fixed effects	Weibull scale (v_l)	v_0	2.800	18.04	23.19
v_1			3.600	-0.09	9.97	94.0 [87.4, 97.8]
Weibull shape (ρ_l)		ρ_0	1.700	-8.38	14.15	88.0 [80.0, 93.6]
		ρ_1	2.800	10.98	19.79	92.0 [84.8, 96.5]

Table 4 Absolute error on the longitudinal outcomes for the Joint cause-specific Spatiotemporal and reference models on PRO-ACT data (Benchmark dataset)

Legend: Joint: the Joint cause-specific Spatiotemporal model, Longitudinal: Spatiotemporal longitudinal model, JMbayes2: joint model with shared random effects with cause-specific survival model estimated using JMbayes2. Results are presented with the mean (SD) over the 10-fold cross-validation. P-values are computed using a Wilcoxon signed-rank test with Bonferroni correction between the Joint Temporal model and each of the reference models. The absolute bias should be minimised and the best results are in bold. 12,197 longitudinal predictions were made at 0.55 (0.47) years from the last visit.

	Joint	Longitudinal	p-value	JMbayes2	p-value
Bulbar	1.187 (1.312)	1.179 (1.301)	2.8e-18	1.166 (1.233)	3.4e-02
Fine motor	1.510 (1.425)	1.499 (1.417)	5.1e-24	1.502 (1.397)	9.8e-01
Gross motor	1.424 (1.331)	1.414 (1.335)	6.5e-30	1.365 (1.288)	6.1e-08



Table 5 Event metrics on NIV initiation and death for the Joint cause-specific Spatiotemporal and reference models on PRO-ACT data (Benchmark dataset)

Legend: NIV: Non Invasive Ventilation initiation, Joint: the Joint Temporal model, Longitudinal: Spatiotemporal longitudinal model, JMbayes2: joint model with shared random effects with cause-specific survival model estimated using JMbayes2.

Results are presented with the mean (SD) over the 10-fold cross-validation. P-values are computed using a Wilcoxon signed-rank test with Bonferroni correction. ↓ means that the metric should be minimised and ↑ maximised. Results in bold are the best for each metric for each event.

	NIV			Death		
	Joint	JMbayes2	p-value	Joint	JMbayes2	p-value
IBS ↓	0.131 (0.013)	0.124 (0.015)	7.8e-03	0.142 (0.02)	0.138 (0.021)	1.3e-06
AUC ↑	0.642 (0.085)	0.633 (0.091)	1.0e+00	0.719 (0.101)	0.695 (0.107)	1.7e-01
C-index 1.0y ↑	0.654 (0.043)	0.632 (0.046)	5.9e-02	0.654 (0.042)	0.637 (0.042)	1.6e-01
C-index 1.5y ↑	0.654 (0.044)	0.642 (0.048)	2.2e-01	0.655 (0.042)	0.642 (0.045)	1.2e-01

APPENDIX

A LIKELIHOOD

Notations

As a reminder, note that there are N patients indexed by i and each has n_i visits indexed by j . Note that $t_0 = \bar{\tau}$. K outcomes and N_s sources and T_e is the time of observation of the event and B_e is the associated boolean whether the event was observed or not (see section 2.2), parameters are defined in section 2.4.1.

Likelihood

The likelihood estimated by the model is the following:

$$p(y, T_e, B_e | \theta, \Pi) = \int_z p(y, T_e, B_e, z | \theta, \Pi) dz$$

$p(y, T_e, B_e, z | \theta, \Pi)$ can be divided into four different terms: the longitudinal data attachment, the survival data attachment and two terms for the prior attachment of latent parameters (fixed and random). We end up with the following expression :

$$\begin{aligned} \log p((y, t_e, B_e), z | \theta, \Pi) &= \log p(y | z, \theta, \Pi) + \log p(t_e, B_e | z, \theta, \Pi) \\ &+ \log p(z_{re} | z_{fe}, \theta, \Pi) + \log p(z_{fe} | \theta, \Pi) \end{aligned}$$

The different parts of the log-likelihood are described below associated with their different assumptions, with the priors attachment to latent fixed effect, $p(z_{fe} | \theta, \Pi)$, separated for longitudinal and survival effects.

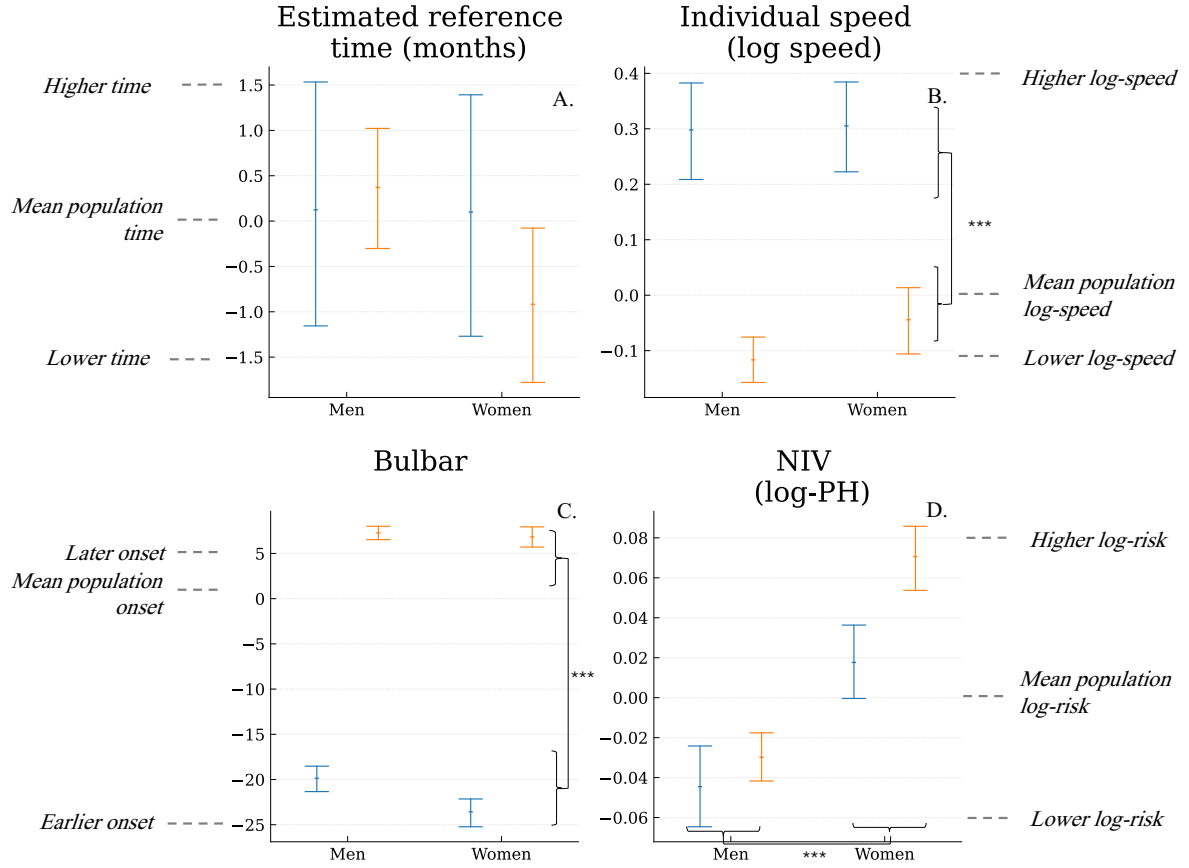


Figure 1 Individual estimated reference time and speed depending on sex and symptom onset

Legend: Graphs present the mean of random effects distribution for the four subgroups defined by sex (in abscissa men, women) and symptom onset (blue: Bulbar, orange: Spinal) with its confidence interval 95%. Panel A: the vertical axis presents the estimated reference time in months compared to the mean estimated reference time of the whole population. Panel B: The vertical axis presents the log speed compared to the mean log speed of the whole population. ANOVA interaction p-value with Bonferroni correction: (A) 1. estimated reference time, (B) 1. individual log-speed.

Longitudinal data attachment

To model the longitudinal process, we assumed that patients and their visits are independent conditionally on random effects and that the noise of the process follows a Gaussian distribution. We thus got (Koval, 2020 p.175):

$$\begin{aligned} \log p(y | z, \theta, \Pi) &= \sum_{i,j,k} \log p(y_{i,j,k} | z, \theta, \Pi) \\ &= \sum_{i,j,k} -\log(\sigma_k \sqrt{2\pi}) - \frac{1}{2\sigma_k^2} (y_{i,j,k} - \gamma_{i,k}(t_{i,j,k}))^2 \end{aligned}$$

Survival data attachment

To model the survival process, we assumed that all patients were independent and that the modelling of the survival process depended on whether the event was observed or not. Note that the following equation could be interpreted as follows: the patient must have survived till the time of observation (or censure) and then has an instantaneous risk for the observed events (Mozumder et al., 2018):

$$\begin{aligned}
\log p(t_e, B_e | z, \theta, \Pi) &= \sum_i \log p(t_{e_i}, B_{e_i} | z, \theta, \Pi) \\
&= \sum_{i,l} \mathbb{1}_{B_{e_i}=l} \times \log (h_{i,l}(t_{e_i})) + \sum_{i,l} \log (S_{i,l}(t_{e_i})) \\
&= \sum_{i,l} \mathbb{1}_{B_{e_i}=l} \times \log \left(\frac{\rho_l e^{\xi_i}}{\nu_l} \left(\frac{e^{\xi_i}(t_{e_i} - \tau_i)}{\nu_l} \right)^{\rho_l - 1} \exp(u_{i,l}) \right) \\
&- \sum_{i,l} \left(\frac{e^{\xi_i}(t_{e_i} - \tau_i)}{\nu_l} \right)^{\rho_l} \exp(u_{i,l})
\end{aligned}$$

The likelihood for a simple event could be extracted from the above formula by putting $L = 1$. If $\psi_i(t) < t_0$ $\log(h_i(t_{e_i})) = -\infty$, to prevent estimation issues, we initialised the algorithm at a possible point getting inspiration from barrier methods (Nesterov, 2018).

Latent random effects priors attachment

As patients were supposed independent of each other, we supposed that random effects were independent conditionally to z_{fe} , θ , and Π . The regularization term associated, with $\bar{\xi} = 0$, $t_0 = \bar{\tau}$, $\bar{s} = 0$ and $\sigma_s = 1$, is then (Koval, 2020 p.175):

$$\begin{aligned}
\log p(z_{re} | z_{fe}, \theta, \Pi) &= \sum_i \left(\log p(\tau_i | z_{fe}, \theta, \Pi) + \log p(\xi_i | z_{fe}, \theta, \Pi) + \sum_m^{N_s} \log p(s_{i,m} | z_{fe}, \theta, \Pi) \right) \\
&= - N \log(\sigma_\tau \sqrt{2\pi}) - \frac{1}{2\sigma_\tau^2} \sum_i (\tau_i - t_0)^2 \\
&- N \log(\sigma_\xi \sqrt{2\pi}) - \frac{1}{2\sigma_\xi^2} \sum_i (\xi_i - \bar{\xi})^2 \\
&- N N_s \log(\sigma_s \sqrt{2\pi}) - \frac{1}{2\sigma_s^2} \sum_i \sum_m^{N_s} (s_{i,m})^2
\end{aligned}$$

Latent fixed effects priors longitudinal attachment

Each longitudinal latent fixed effect is independently sampled from a posterior distribution. The regularization term associated is then (Koval, 2020 p.175):

$$\begin{aligned}
\log p(z_{fe} | \theta, \Pi) &= \sum_k (\log p(\tilde{g}_k | \theta, \Pi) + \log p(\tilde{v}_{0,k} | \theta, \Pi)) \\
&+ \sum_{o,m} \log p(\beta_{o,m} | \theta, \Pi) \\
&= - \sum_k \log(\sigma_{\tilde{g}} \sqrt{2\pi}) - \frac{1}{2\sigma_{\tilde{g}}^2} (\tilde{g}_k - \bar{g}_k)^2 \\
&- \sum_k \log(\sigma_{\tilde{v}_0} \sqrt{2\pi}) - \frac{1}{2\sigma_{\tilde{v}_0}^2} (\tilde{v}_{0,k} - \bar{v}_{0,k})^2 \\
&- (K-1)N_s \log(\sigma_{\beta} \sqrt{2\pi}) - \frac{1}{2\sigma_{\beta}^2} \sum_{o,m} (\beta_{o,m} - \bar{\beta}_{o,m})^2
\end{aligned}$$

Latent fixed effects prior event attachment

Each latent fixed effect is independently sampled from a posterior distribution. The regularization term associated is then:

$$\begin{aligned}
\log p(\tilde{v}, \tilde{\rho}, \zeta | \theta, \Pi) &= \sum_l \log p(\tilde{v}_l | \theta, \Pi) + \log p(\tilde{\rho}_l | \theta, \Pi) \\
&+ \sum_{l,m} \log p(\zeta_{l,m} | \theta, \Pi) \\
&= - \sum_l \log(\sigma_{\tilde{v}_l} \sqrt{2\pi}) - \frac{1}{2\sigma_{\tilde{v}_l}^2} (\tilde{v}_l - \bar{v}_l)^2 \\
&- \sum_l \log(\sigma_{\tilde{\rho}_l} \sqrt{2\pi}) - \frac{1}{2\sigma_{\tilde{\rho}_l}^2} (\tilde{\rho}_l - \bar{\rho}_l)^2 \\
&- \sum_{l,m} \log(\sigma_{\zeta} \sqrt{2\pi}) - \frac{1}{2\sigma_{\zeta}^2} (\zeta_{l,m} - \bar{\zeta}_{l,m})^2
\end{aligned}$$

Total formula

$$\begin{aligned}
\log p((y, T_e, B_e), z, \theta | \Pi) = & \sum_{i,j,k} -\log(\sigma_k \sqrt{2\pi}) - \frac{1}{2\sigma_k^2} (y_{i,j,k} - \gamma_{i,k}(t_{i,j,k}))^2 \\
+ & \sum_{i,l} \mathbb{1}_{B_{e_i}=l} \times \log(h_{i,l}(t_{e_i})) + \sum_{i,l} \log(S_{i,l}(t_{e_i})) \\
- & \sum_k \log(\sigma_{\tilde{g}} \sqrt{2\pi}) - \frac{1}{2\sigma_{\tilde{g}}^2} (\tilde{g}_k - \bar{\tilde{g}}_k)^2 \\
- & \sum_k \log(\sigma_{\tilde{v}_0} \sqrt{2\pi}) - \frac{1}{2\sigma_{\tilde{v}_0}^2} (\tilde{v}_{0,k} - \bar{\tilde{v}}_{0,k})^2 \\
- & \sum_l \log(\sigma_{\tilde{v}} \sqrt{2\pi}) - \frac{1}{2\sigma_{\tilde{v}}^2} (\tilde{v}_l - \bar{v}_l)^2 \\
- & \sum_l \log(\sigma_{\tilde{\rho}} \sqrt{2\pi}) - \frac{1}{2\sigma_{\tilde{\rho}}^2} (\tilde{\rho}_l - \bar{\rho}_l)^2 \\
- & (K-1)N_s \log(\sigma_{\beta} \sqrt{2\pi}) - \frac{1}{2\sigma_{\beta}^2} \sum_{o,m} (\beta_{o,m} - \bar{\beta}_{o,m})^2 \\
- & LN_s \log(\sigma_{\zeta} \sqrt{2\pi}) - \frac{1}{2\sigma_{\zeta}^2} \sum_{l,m} (\tilde{\zeta}_{l,m} - \bar{\zeta}_{l,m})^2 \\
- & N \log(\sigma_{\tau} \sqrt{2\pi}) - \frac{1}{2\sigma_{\tau}^2} \sum_i (\tau_i - \bar{\tau})^2 \\
- & N \log(\sigma_{\xi} \sqrt{2\pi}) - \frac{1}{2\sigma_{\xi}^2} \sum_i (\xi_i - \bar{\xi})^2 \\
- & NN_s \log(\sigma_s \sqrt{2\pi}) - \frac{1}{2\sigma_s^2} \sum_i \sum_m^{N_s} (s_{i,m} - \bar{s})^2
\end{aligned}$$

B SUFFICIENT STATISTICS

The convergence of the Monte-Carlo Markov Chain Stochastic Approximation Expectation-Maximization (MCMC-SAEM) algorithm has been proven in Kuhn and Lavielle, 2004 for models which lie into the curved exponential family. For such a family of distributions, the log-likelihood can be written as:

$$\log p(Y, z, \theta, \Pi) = -\Phi(\theta, \Pi) + \langle S(Y, z), f(\theta, \Pi) \rangle + A(Y, z, \Pi)$$

where Φ and f are smooth functions, and S are called the sufficient statistics. The sufficient statistics are to be understood as a summary of the required information from the latent variables z and the observations Y . Our models fall in such a category and sufficient statistics are described below. Note that for the joint models, the same kind of decomposition was done by Lavalley-Morelle et al., 2024.

The idea is to rewrite likelihood in the above form to get sufficient statistics. As a reminder, note that there are N patients indexed by i and each has visits indexed by j .

$$\begin{aligned}
\log q((y, T_e, B_e), z, \theta \mid \Pi) = & - \sum_{i,j,k} \ln(\sigma_k \sqrt{2\pi}) - \underbrace{\langle [\|y_{ij}\|^2]_{ij} \rangle}_{S_1(y,z)} - 2 \underbrace{[y_{ij}^T \gamma_i(t_{i,j})]_{ij}}_{S_2(y,z)} + \underbrace{\langle [\|\gamma_i(t_{i,j})\|^2]_{ij} \rangle}_{S_3(y,z)} \frac{1}{2[\sigma_k^2]_k} \mathbf{1}_{\Sigma_{i,j,k} 1} \rangle \\
& + \left[\sum_{i,l} \mathbb{1}_{B_{e_i}=l} \times \log(h_{i,l}(t_{e_i})) + \sum_{i,l} \log(S_{i,l}(t_{e_i})) \right]_i, \\
& - KN \ln(\sigma_{\tilde{v}_0} \sqrt{2\pi}) - \sum_{k=1}^K \frac{1}{2\sigma_{\tilde{v}_0}^2} \tilde{v}_{0k}^2 + \underbrace{\langle [\tilde{v}_{0,k}^2]_k \rangle}_{S_4(y,z)} - \frac{1}{2\sigma_{\tilde{v}_0}^2} \mathbf{1}_K \rangle + \underbrace{\langle [\tilde{v}_{0,k}]_k \rangle}_{S_5(y,z)} \frac{1}{\sigma_{\tilde{v}_0}^2} \langle [\tilde{v}_{0k}]_k \rangle \\
& - K \ln(\sigma_{\tilde{g}} \sqrt{2\pi}) - \sum_{k=1}^K \frac{1}{2\sigma_{\tilde{g}}^2} \tilde{g}_k^2 + \underbrace{\langle [\tilde{g}_k^2]_k \rangle}_{S_6(y,z)} - \frac{1}{2\sigma_{\tilde{g}}^2} \mathbf{1}_K \rangle + \underbrace{\langle [\tilde{g}_k]_k \rangle}_{S_7(y,z)} \frac{1}{\sigma_{\tilde{g}}^2} \langle [\tilde{g}_k]_k \rangle \\
& - (K-1)N_s \ln(\sigma_\beta \sqrt{2\pi}) - \sum_{o,m} \frac{1}{2\sigma_\beta^2} \tilde{\beta}_{o,m}^2 \\
& + \underbrace{\langle [\beta_{o,m}^2]_{o,m} \rangle}_{S_8(y,z)} - \frac{1}{2\sigma_\beta^2} \mathbf{1}_{(K-1)N_s} \rangle + \underbrace{\langle [\beta_{o,m}]_{o,m} \rangle}_{S_9(y,z)} \frac{1}{\sigma_\beta^2} \langle [\tilde{\beta}_{o,m}]_{o,m} \rangle \\
& - \ln(\sigma_{\tilde{v}} \sqrt{2\pi}) - \sum_{l=1}^L \frac{1}{2\sigma_{\tilde{v}}^2} \tilde{v}_l^2 + \underbrace{\langle [\tilde{v}_l^2]_l \rangle}_{S_{10}(Y,z)} - \frac{1}{2\sigma_{\tilde{v}}^2} \mathbf{1}_1 \rangle + \underbrace{\langle [\tilde{v}_l]_l \rangle}_{S_{11}(Y,z)} \frac{1}{\sigma_{\tilde{v}}^2} \langle [\tilde{v}_l]_l \rangle \\
& - \ln(\sigma_{\tilde{\rho}} \sqrt{2\pi}) - \sum_{l=1}^L \frac{1}{2\sigma_{\tilde{\rho}}^2} \tilde{\rho}_l^2 + \underbrace{\langle [\tilde{\rho}_l^2]_l \rangle}_{S_{12}(Y,z)} - \frac{1}{2\sigma_{\tilde{\rho}}^2} \mathbf{1}_1 \rangle + \underbrace{\langle [\tilde{\rho}_l]_l \rangle}_{S_{13}(Y,z)} \frac{1}{\sigma_{\tilde{\rho}}^2} \langle [\tilde{\rho}_l]_l \rangle \\
& - LN_s \ln(\sigma_\zeta \sqrt{2\pi}) - \sum_{l,m} \frac{1}{2\sigma_\zeta^2} \tilde{\zeta}_{l,m}^2 \\
& + \underbrace{\langle [\zeta_{l,m}^2]_{l,m} \rangle}_{S_{14}(y,z)} - \frac{1}{2\sigma_\zeta^2} \mathbf{1}_{LN_s} \rangle + \underbrace{\langle [\zeta_{l,m}]_{l,m} \rangle}_{S_{15}(y,z)} \frac{1}{\sigma_\zeta^2} \langle [\tilde{\zeta}_{l,m}]_{l,m} \rangle \\
& - N \log(\sigma_\tau \sqrt{2\pi}) - \frac{1}{2\sigma_\tau^2} N \tilde{\tau}^2 + \underbrace{\langle [\tau_i^2]_i \rangle}_{S_{16}(Y,z)} - \frac{1}{2\sigma_\tau^2} \mathbf{1}_N \rangle + \underbrace{\langle [\tau_i]_i \rangle}_{S_{17}(Y,z)} \frac{1}{\sigma_\tau^2} \langle \tilde{\tau} \mathbf{1}_N \rangle \\
& - N \log(\sigma_\xi \sqrt{2\pi}) - \frac{1}{2\sigma_\xi^2} N \tilde{\xi}^2 + \underbrace{\langle [\xi_i^2]_i \rangle}_{S_{18}(Y,z)} - \frac{1}{2\sigma_\xi^2} \mathbf{1}_N \rangle + \underbrace{\langle [\xi_i]_i \rangle}_{S_{19}(Y,z)} \frac{1}{\sigma_\xi^2} \langle \tilde{\xi} \mathbf{1}_N \rangle \\
& - NN_s \log(\sigma_s \sqrt{2\pi}) - N \sum_{m=1}^{N_s} \frac{1}{2\sigma_s^2} \tilde{s}_m^2 \\
& + \underbrace{\langle [\tilde{s}_{il}^2]_{il} \rangle}_{S_{20}(y,z)} - \frac{1}{2\sigma_s^2} \mathbf{1}_{NN_s} \rangle + \sum_{m=1}^{N_s} \underbrace{\langle [\tilde{s}_{im}]_i \rangle}_{S_{21}(y,z)} \frac{1}{\sigma_s^2} \langle [\tilde{s}] \rangle
\end{aligned}$$

C MAXIMIZATION UPDATE RULES

To find the update rule of the different parameters, we need to find the new parameter θ that maximizes the log-likelihood. As expressions are convex in θ we can simply derive and look for a critical point. We derive the log-likelihood with respect to each maximised fixed effect. Note that only maximised fixed effects are updated by a maximization rule, other parameters are latent variables that are sampled. $\bar{\xi}$ is first maximised and then set to 0 and $\bar{s} = 0$ and $\sigma_s = 1$. As a reminder, note that there are N patients indexed by i and that each of them has n_i visits indexed by j . At iteration c , we can use $\tilde{S}^{(c+1)}$ computed with the parameters at iteration c and the formula of $S(Y, z)$ to compute the parameters at iteration $(c + 1)$.

See notation in section 2.2 and parameters in section 2.4.1, and sufficient statistics section B

$$\begin{aligned}
(\sigma^2)^{(c+1)} &\leftarrow \frac{1}{N} [\tilde{S}_1^{(c+1)} - 2\tilde{S}_2^{(c+1)} + \tilde{S}_3^{(c)}]^T \mathbf{1}_1 \\
(\bar{v}_{0k})^{c+1} &\leftarrow \tilde{S}_5^{(c+1)} \\
(\bar{g}_k)^{c+1} &\leftarrow \tilde{S}_7^{(c+1)} \\
(\bar{\beta}_{o,m})^{c+1} &\leftarrow \tilde{S}_9^{(c+1)} \\
(\bar{v}_l)^{(c+1)} &\leftarrow \tilde{S}_{11}^{(c+1)} \\
(\bar{\rho}_l)^{(c+1)} &\leftarrow \tilde{S}_{13}^{(c+1)} \\
(\bar{\zeta}_{l,m})^{c+1} &\leftarrow \tilde{S}_{15}^{(c+1)} \\
(\bar{\tau})^{(c+1)} &\leftarrow \frac{1}{N} \tilde{S}_{17}^{(c+1)} \\
(\sigma_\tau^2)^{(c+1)} &\leftarrow \frac{1}{N} [\tilde{S}_{16}^{(c+1)} - 2\bar{\tau} \tilde{S}_{17}^{(c+1)}]^T \mathbf{1}_N + \bar{\tau}^2 \\
(\bar{\xi})^{(c+1)} &\leftarrow \frac{1}{N} \tilde{S}_{19}^{(c+1)} \\
(\sigma_\xi^2)^{(c+1)} &\leftarrow \frac{1}{N} [\tilde{S}_{18}^{(c+1)} - 2\bar{\xi} \tilde{S}_{19}^{(c+1)}]^T \mathbf{1}_N + \bar{\xi}^2
\end{aligned}$$

D JACOBIAN LIKELIHOOD

To faster personalisation, gradients are computed for $\xi_i \times \sigma_\xi$ and $\tau_i \times \sigma_\tau$. Thus all the equations must be multiplied by the standard deviation at the end, to get the implemented formulas.

D.1 Longitudinal data attachment

From likelihood

Longitudinal noise is supposed to follow Gaussian law, we have to derive the following quantity per patient i and visit j for the outcome k :

$$\log p(y_{i,j,k} \mid z, \theta, \Pi) = -\log \left(\sigma_k \sqrt{2\pi} \right) - \frac{1}{2\sigma_k^2} (y_{i,j,k} - \gamma_{i,k}(t_{i,j,k}))^2$$

Jacobian

Using the known formula of the derivative of the logistic function, we get:

$$\begin{aligned} C_{i,j,k} &= \frac{(1+g_k)^2}{g_k} [y_{i,j,k} - \gamma_{i,k}(t_{i,j,k})] [\gamma_{i,k}(t_{i,j,k})] [1 - \gamma_{i,k}(t_{i,j,k})] \\ \frac{\partial \log p(y_{i,j,k} | z, \theta, \Pi)}{\partial \xi_i} &= \frac{1}{\sigma^2} (v_{0,k} \psi_i(t_{i,j,k}) \times C_{i,j,k}) \\ \frac{\partial \log p(y_{i,j,k} | z, \theta, \Pi)}{\partial \tau_i} &= -\frac{1}{\sigma^2} (v_{0,k} e^{\xi_i} \times C_{i,j,k}) \\ \frac{\partial \log p(y_{i,j,k} | z, \theta, \Pi)}{\partial s_{i,m}} &= -\frac{1}{\sigma^2} (A_{k,m} \times C_{i,j,k}) \end{aligned}$$

D.2 Survival data attachment

From likelihood

On the other side, the modelling of the survival process depends on whether the event is observed or not for each patient i :

$$\begin{aligned} \log p(t_{e_i}, B_{e_i} | z, \theta, \Pi) &= \sum_l \mathbb{1}_{B_{e_i}=l} \times \log \left(\frac{\rho_l e^{\xi_i}}{v_l} \left(\frac{e^{\xi_i}(t_{e_i}-\tau_i)}{v_l} \right)^{\rho_l-1} \exp \left(\sum_m \zeta_{l,m} s_{i,m} \right) \right) \\ &\quad - \sum_l \left(\frac{e^{\xi_i}(t_{e_i}-\tau_i)}{v_l} \right)^{\rho_l} \exp \left(\sum_m \zeta_{l,m} s_{i,m} \right) \end{aligned}$$

Jacobian

We thus get:

$$\begin{aligned} \frac{\partial \log q(t_{e_i}, B_{e_i} | z, \theta, \Pi)}{\partial \xi_i} &= \sum_l \mathbb{1}_{B_{e_i}=l} \rho_l - \rho_l \times \left(\frac{\psi_l(t_{e_i})}{v_l} \right)^{\rho_l} \exp \left(\sum_m \zeta_{l,m} s_{i,m} \right) \\ &= \sum_l \mathbb{1}_{B_{e_i}=l} \rho_l + \rho_l \times \log \left(S_{i,l}(t_{e_i}) \right) \\ \frac{\partial \log q(t_{e_i}, B_{e_i} | z, \theta, \Pi)}{\partial \tau_i} &= \sum_l -\frac{(\rho_l-1)}{(t_{e_i}-\tau_i)} \mathbb{1}_{B_{e_i}=l} - \frac{\rho_l e^{\xi_i}}{v_l} \left(\frac{\psi_l(t_{e_i})}{v_l} \right)^{\rho_l-1} \exp \left(\sum_m \zeta_{l,m} s_{i,m} \right) \\ &= \sum_l -\frac{(\rho_l-1)}{(t_{e_i}-\tau_i)} \mathbb{1}_{B_{e_i}=l} - h_{i,l}(t_{e_i}) \\ \frac{\partial \log q(t_{e_i}, B_{e_i} | z, \theta, \Pi)}{\partial s_{i,m}} &= \sum_l \mathbb{1}_{B_{e_i}=l} \zeta_{l,m} - \zeta_{l,m} \times \left(\frac{\psi_l(t_{e_i})}{v_l} \right)^{\rho_l} \exp \left(\sum_m \zeta_{l,m} s_{i,m} \right) \\ &= \sum_l \mathbb{1}_{B_{e_i}=l} \zeta_{l,m} + \zeta_{l,m} \times \log \left(S_{i,l}(t_{e_i}) \right) \end{aligned}$$

D.3 Random effects regularisation

From likelihood

$$\begin{aligned} \log p(z_{re} | \theta, \Pi) &= -N \log \left(\sigma_\tau \sqrt{2\pi} \right) - \frac{1}{2\sigma_\tau^2} \sum_i (\tau_i - \bar{\tau})^2 \\ &- N \log \left(\sigma_\xi \sqrt{2\pi} \right) - \frac{1}{2\sigma_\xi^2} \sum_i (\xi_i - \bar{\xi})^2 \\ &- N N_s \log \left(\sigma_s \sqrt{2\pi} \right) - \frac{1}{2\sigma_s^2} \sum_i \sum_m^{N_s} (s_{i,m} - \bar{s})^2 \end{aligned}$$

Jacobian

We thus get:

$$\begin{aligned}\frac{\partial \log q(\xi_i | \theta, \Pi)}{\partial \xi_i} &= \left(\frac{\xi_i - \bar{\xi}}{\sigma_\xi} \right) \\ \frac{\partial \log q(\tau_i | \theta, \Pi)}{\partial \tau_i} &= \left(\frac{\tau_i - \bar{\tau}}{\sigma_\tau} \right) \\ \frac{\partial \log q(s_{i,m} | \theta, \Pi)}{\partial s_{i,m}} &= \left(\frac{s_{i,m} - \bar{s}}{\sigma_s} \right)\end{aligned}$$

E MATERIAL COMPLEMENTARY

E.1 Event extraction

Death

All the deaths were stored in one file. For patients without observed death, we censored their deaths with the date of the last visit.

Tracheostomy

Tracheostomy is a medical intervention, some codes were available in one of the tables using the Medical Dictionary for Regulatory Activities (MDRA). After analysis of the different labels, we have decided to keep the Lowest Level Term, displayed in Figures E1, to extract an exact date of tracheostomy. Information on tracheostomy is also available in item 12 of ALSFRS_r. For patients with no information from the medical intervention table, we extracted interval-censored events.

Non-Invasive Ventilation (NIV)

Non-Invasive Ventilation (NIV) was not coded medical intervention table but was coded in item 12 of ALSFRS_r and item 10 of ALSFRS. We were thus able to extract interval-censored data.

E.2 Simulated scenario

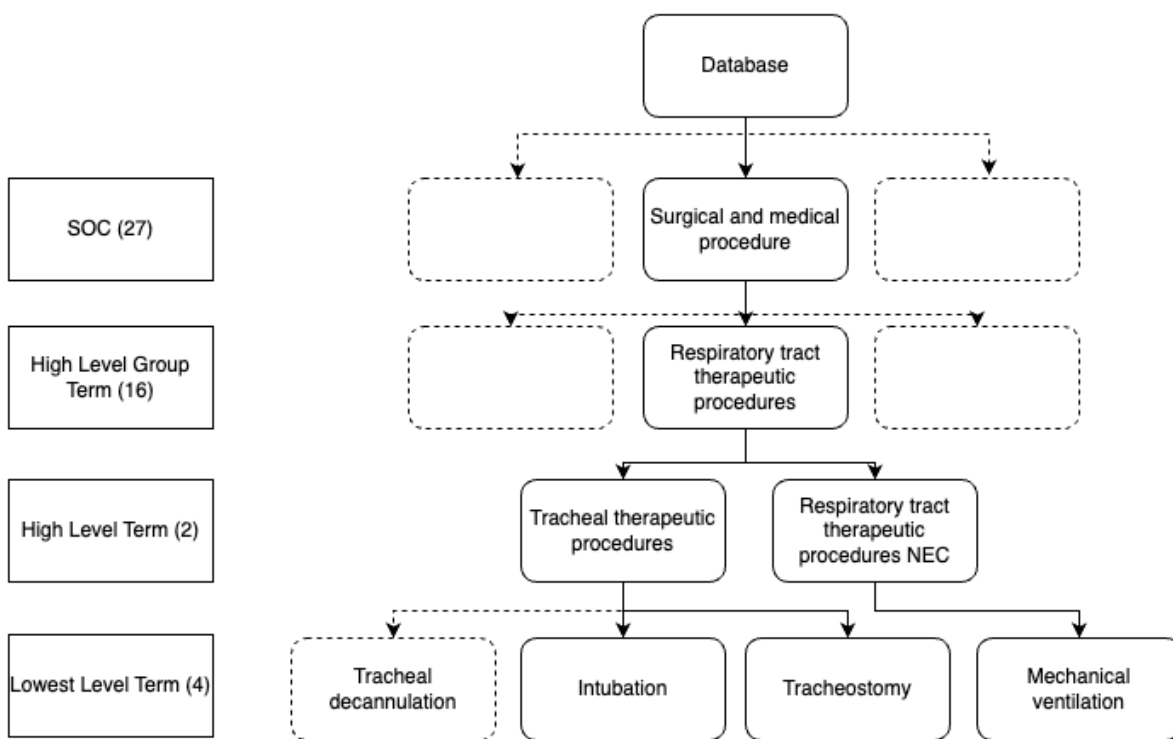


Figure E1 Medical intervention terms related to tracheostomy using Medical Dictionary for Regulatory Activities (MDRA)

Legend: SOC: Standard Of Care, each square represents a level in the medical intervention terms tree, the numbers in parentheses are the numbers of possible terms at each level of the tree, not selected levels and terms are represented with dashed

Table E1 Data simulation parameters by scenario

Legend: Real-like: Real-like simulated dataset (valid shared latent age hypothesis), No link: No-link dataset (invalid shared latent age hypothesis), (r) indicate when ALS real-like parameters are used. More information on simulation is available in section 3.2. $\bar{\tau} = t_0, \bar{\xi} = 0, \sigma_s = 1$ and $\bar{s} = 0$

Type	Parameters Name		Symbol	Estimated parameters (r)	Real-like simulation	No-link simulation
Patients	Patient number		N	300	r	r
Random Effect	Population estimated reference time (year)	(mean)	$\bar{\tau}$	5.00	r	r
		(std)	σ_{τ}	1.100	r	r
	Individual log-speed factor	(mean)	$\bar{\xi}$	0	r	r
		(std)	σ_{ξ}	0.790	r	r
	Number of sources		N_s	2	r	r
Longitudinal Fixed Effects	Speed of the logistic curve		ν_0	[0.069, 0.188, 0.198, 0.112]	r	r
	Curve value at t_0 : $\frac{1}{1+g}$		g	[13.958, 5.316, 3.993, 5.704]	r	r
	Estimated noise		σ	[0.07, 0.08, 0.07, 0.04]	[25, 15, 16, 75]	[25, 15, 16, 75]
	Longitudinal mixing matrix		A	[[0.059, -0.103, 0.001, 0.004], [0.059, 0.006, -0.141, -0.004]]	[[0.06, -0.10, 0.00, 0.01], [0.06, 0.006, -0.14, -0.00]]	[[0.06, -0.10, 0.00, 0.01], [0.06, 0.01, -0.14, -0.00]]
Survival Fixed Effects	Scale of the Weibull distribution		ν	[3.4, 3.9]	[2.8, 3.6]	[2.8, 3.6]
	Shape of the Weibull distribution		ρ	[1.7, 2.8]	r	r
	Hazard ratio coefficients		ζ	[[-0.09, 0.09] [-0.1, 0.05]]	[[-0.09, 0.09] [-0.1, 0.0]]	[[-0.09, 0.09] [-0.1, 0.0]]
Visits	Time between τ and baseline (years)	(mean)	$\bar{\delta}_b$	0.2	0.	0.
		(std)	σ_{δ_b}	0.4	0.4	0.4
	Time of follow up (year)	(mean)	\bar{T}_f	0.8	1.1	1.1
		(std)	σ_{T_f}	0.5	r	r
	Time between visits (months)	(mean)	$\bar{\delta}_v$	1.4	2.0	2.0
		(std)	σ_{δ_v}	0.75	r	r

F SIMULATION STUDY COMPLEMENTARY

Table F2 Intraclass correlation of random effects of the Joint cause-specific Spatiotemporal model estimated on the Real-like dataset

Legend: Mean intraclass correlation with the standard deviation over the simulated scenario (SD).

Random effects			Intraclass correlation
Log-speed factor	ξ_i		0.844 (0.020)
Individual estimated reference time	τ_i		0.919 (0.020)
Space shifts	Bulbar	$w_{i,0}$	0.967 (0.006)
	Fine motor	$w_{i,1}$	0.939 (0.009)
	Gross motor	$w_{i,2}$	0.954 (0.007)
	Total	$w_{i,3}$	0.904 (0.042)
Survival shifts	VNI	$u_{i,0}$	0.479 (0.416)
	Death	$u_{i,1}$	0.147 (0.445)

G APPLICATION STUDY

Table G3 Comparison of the parameters estimated by the Joint cause-specific Spatiotemporal model with the one estimated by the cause-specific AFT model on PROACT data (analysis dataset)

Legend: NIV: Non Invasive Ventilation initiation, Parameters: parameters of the Weibull distribution with the matched scale (nu for the AFT model and $nu+t_0$ for the joint model with t_0 the estimated reference time), ρ the shape, Joint Spatiotemporal: Joint cause-specific Spatiotemporal model, Cause-specific AFT: Cause-specific Accelerate Failure Time model.

	Matched weibull scale Relative difference (%)	Weibull shape		
		Spatiotemporal (ρ_l)	Cause-specific AFT(ρ_l)	Concordance of hazard progression
NIV	-5.12	1.91	2.1 [1.9, 2.2]	yes
Death	-22.28	3.50	2.3 [2.1, 2.6]	yes

G.1 Individual spatial variability

Motor decline ($w_i v_0^{-1}$)

We found an interaction between sex and onset site for gross motor ($p = 0.034$) but not for fine motor scales (p -value = 1.), once corrected for the estimated reference timing and speed of progression (Figure G3 A and B).

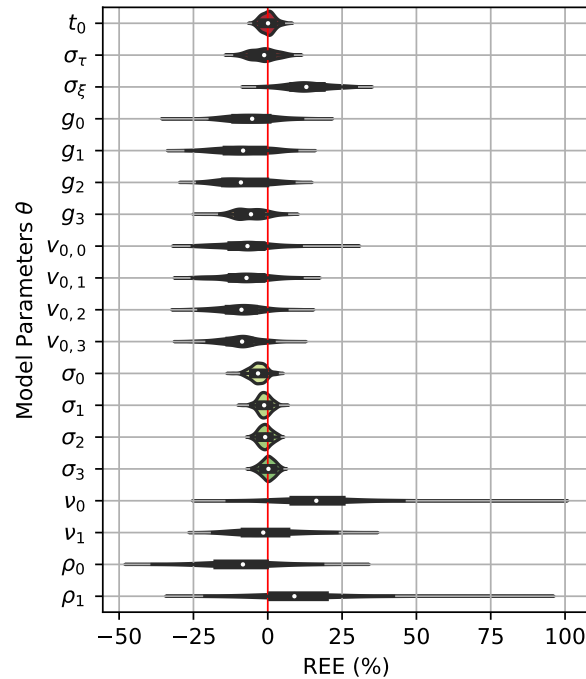


Figure F2 Relative Estimation Error on the simulated real-like datasets

Legend: Distribution over the 100 real-like simulated datasets, t_0 : Estimated reference time (mean), σ_τ : Estimated reference time (std), σ_ξ : Individual log-speed factor (std), g_k : Curve values at $t_0 \left(\frac{1}{1+g_k} \right)$, $v_{0,k}$: Speed of the logistic curves, σ_k : Estimated noises, ν_i : Weibull scale, ρ_i : Weibull shape. Note that: $\bar{\tau} = t_0$, $\bar{\xi} = 0$, $\sigma_s = 1$ and $\bar{s} = 0$

ALSFRSr gross motor scale deteriorated 2.3 months later (95% CI = [1.6, 3.0]) in women than in men. However, ALSFRSr fine motor scale deteriorated 2.4 months earlier (95% CI = [1.9, 2.9]) in women than in men, independently of the onset site.

ALSFRSr gross motor scale deteriorated 11.3 months earlier (95% CI = [10.5, 12.0]) for patients with spinal onset compared to bulbar onset. ALSFRSr fine motor scale deteriorated 10.2 months earlier (95% CI = [9.0, 11.3]) for patients with spinal onset compared to bulbar onset, independently of the sex.

Bulbar signs decline ($w_i v_0^{-1}$)

We did not observe any interaction between sex and onset site for ALSFRSr bulbar scale (p-value = 0.15), once corrected for the estimated reference timing and speed of progression (Figure G3 C).

ALSFRSr bulbar scale deteriorated 28.6 months later (95% CI = [27.4, 29.8]) for patients with spinal onset compared to bulbar onset, independently of the sex.

Non-Invasive Ventilation Initiation (u_i)

After correction for speed and onset, women had a significantly higher risk of NIV initiation compared to men (PH: 1.09 [1.08, 1.11]) (Figure G4 A).

Table G4 Estimated parameters of the Joint cause-specific Spatiotemporal model on the Analysis dataset

Legend: $\bar{\xi}$, \bar{s} , σ_s parameters are not present as they are fixed by the model ($\bar{\xi} = 0$, $\bar{s} = 0$, $\sigma_s = 1$) and $t_0 = \bar{\tau}$

Parameters name		Estimated		
Distribution of random effects	Estimated reference time (mean)	t_0	0.889	
	Estimated reference time (std)	σ_τ	0.974	
	Individual log-speed factor (std)	σ_ξ	0.782	
Longitudinal fixed effects	Curve values at $t_0: \frac{1}{1+g} (g_k)$	bulbar	g_0	25.777
		fine motor	g_1	10.345
		gross motor	g_2	6.945
	Speed of the logistic curves ($v_{0,k}$)	bulbar	$v_{0,0}$	0.039
		fine motor	$v_{0,1}$	0.117
		gross motor	$v_{0,2}$	0.139
	Estimated noises (σ_k)	bulbar	σ_0	0.063
		fine motor	σ_1	0.075
		gross motor	σ_2	0.074
Survival fixed effects	Weibull scale (v_l)	NIV	v_0	3.76
		Death	v_1	4.24
	Weibull shape (ρ_l)	NIV	ρ_0	1.91
		Death	ρ_1	3.50

Death (u_i)

Again, after correction for speed and onset, women had a significantly higher risk of death compared to men (PH: 1.21 [1.16, 1.25]) (Figure G4 B).

H HYPERPARAMETERS SELECTION

H.1 Method

Aims

The number of sources is a hyperparameter that can be adjusted. It corresponds to the number of dimensions allowed for the dimension reduction of the ordering of the longitudinal outcomes (spatial aspect). We wanted to evaluate a method to select the number of sources.

Data generating mechanism

We use the first dataset simulated over the 100 real-like simulated datasets (see 3.2). It was simulated with two sources and four outcomes to unable to tests for 1, 2 and 3 sources (see section 2.3.1).

Estimands

We ran the model for 50,000 iterations with a 10,000 Robbins-Monro convergence phase. We used the fixed effects extracted after the Robbins-Monro convergence phase and for the random effect the mean value over the last 100 iterations.

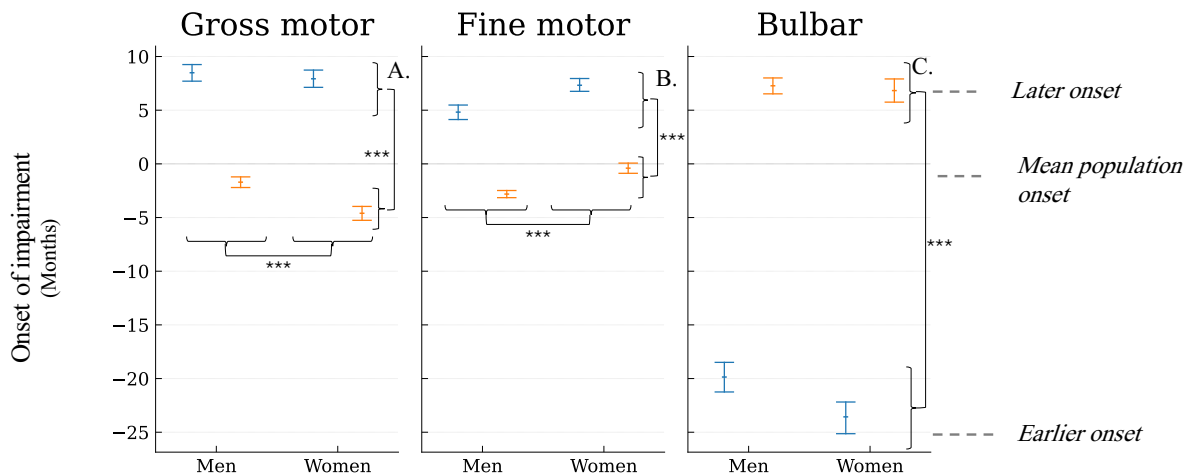


Figure G3 Individual spatial variability on Longitudinal outcomes

Legend: Graphs present the mean of random effects distribution for the four subgroups defined by sex (in abscissa men, women) and symptom onset (blue: Bulbar, orange: Spinal) with its confidence interval 95%. The vertical axis presents the delay of outcome impairment onset in months compared to the mean onset of the whole population. ANOVA interaction p -value with Bonferroni correction: (A) 0.091 gross motor scale, (B) 1. fine motor scale, (C) 0.15 bulbar scale.

Performance metrics

To compare the models, we used the BIC extended for mixed effects models (Delattre et al., 2014). We then kept the number of sources that enabled to minimise the BIC.

H.2 Results

On the Real-like dataset, the BIC was lower for the model with two sources (-13,368) compared to the one with one (-11,922) and three (-11,499) sources.

H.3 Conclusion

These results confirmed what was expected as we simulated data with two sources and thus validated the use of the BIC to select the number of sources.

I LATENT AGE HYPOTHESIS

I.1 Method

I.1.1 Aims

We wanted to give future users tools to evaluate if the shared latent age hypothesis was realistic on their dataset.

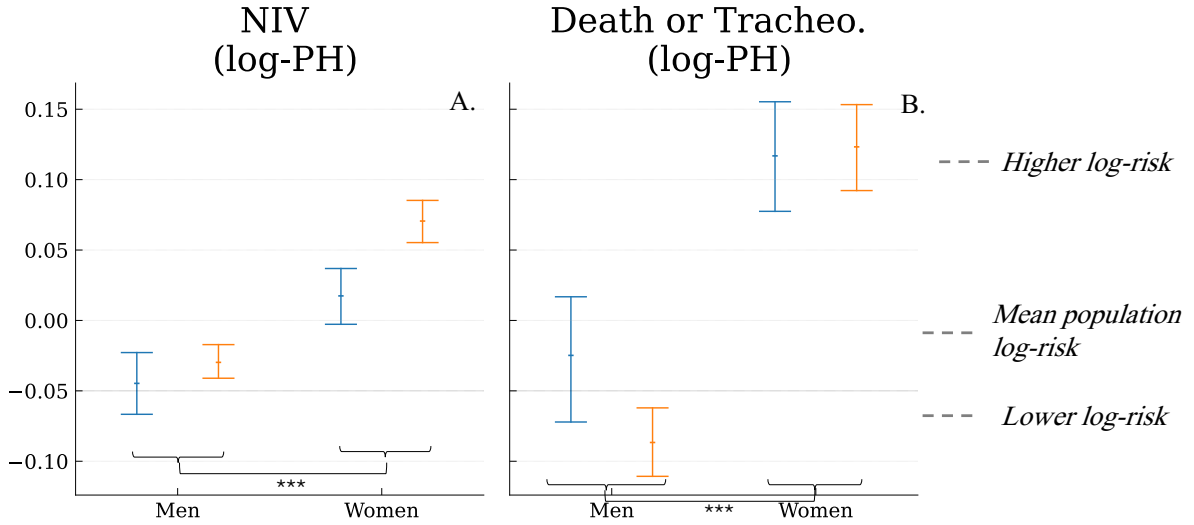


Figure G4 Individual spatial variability on NIV initiation and death

Legend: Graphs present the mean of random effects distribution for the four subgroups defined by sex (in abscissa men, women) and symptom onset (blue: Bulbar, orange: Spinal) with its confidence interval 95%. The vertical axis presents the log Proportional effect of survival shifts on the Hazard compared to the mean of the whole population. ANOVA interaction p-value with Bonferroni correction: (A) 1. NIV initiation log-PH, (B) 1. death

I.2 Data-generating mechanism

We used the first dataset simulated over the 100 of the simulation study, we will refer to it after as the real-like dataset. And use the same parameters to simulate not correlated longitudinal and survival outcomes, referred to as the no-link dataset.

I.2.1 Estimands

We compared the estimated fixed effects from the Joint cause-specific Spatiotemporal model with the one of the cause-specific AFT model and the Longitudinal Spatiotemporal model, both on the real-like and no-link simulated dataset. For survival process, we matched the Weibull scale of the the cause-specific AFT model (ν) with the population estimated reference time plus the Weibull scale of Joint cause-specific Spatiotemporal model ($t_0 + \nu$). Indeed, in the Joint cause-specific Spatiotemporal model the survival submodel starts from t_0 (see section 2.3.3).

I.2.2 Performance metrics

We report the relative difference of the fixed effects of the Joint cause-specific Spatiotemporal model compared to the one of Longitudinal Spatiotemporal model ($\frac{\theta_{long} - \theta_{joint}}{\theta_{joint}}$).

For the Weibull matched scale we reported also the relative difference to AFT model. Depending on the value of the shape of the Weibull distribution (ρ) the hazard function $h(t)$ has different progressions (Jiang and Murthy, 2011):

- $\rho < 1$: indicates that the hazard function decreases over time, which happens if the event is more likely to occur at the beginning of the disease,

- $\rho = 1$: indicates that the hazard function is constant over time, which might suggest random external events are causing the event,
- $\rho > 1$: indicates that the hazard function increases with time, which happens when the event is more likely to happen as time goes on.

So we reported the value of the Weibull shapes and assess if they correspond to the same tendency on the hazard function.

I.3 Results

The two datasets have similar characteristics even if the no-link datasets have slightly less events (Table I5). For the longitudinal parameters relative differences, no major differences were observed and for both datasets are below 25% in absolute value (I6). For the matched survival scale, relative differences was of the same magnitude (below 25% in absolute value) on the real-like dataset but above 100% on the no link dataset (I7). The hazard progression described by the Weibull shape was concordant between the Joint Spatiotemoral model and the AFT model on the real-like dataset but not on the no-link dataset (I7).

I.4 Conclusion

In conclusion, to assess the shared latent disease age between the survival and the longitudinal process, the parameters of the survival submodel seemed more sensible. This could be link to the fact that the survival attachment is less important due to few events compared to the one with the longitudinal data. A really different value of the matched Weibull scale and a hazard progression (drove by the Weibull shape) not concordant between the Joint model and the AFT model could be a good sign of an invalid shared latent age hypothesis.

Table I5 Characteristics of the simulated datasets used to test the shared latent disease age hypothesis

Legend: Results are presented with mean (SD) [class%]. Real-like: Real-like simulated dataset (valid shared latent age hypothesis), No-link: No link dataset (invalid shared latent age hypothesis)

Type	Characteristics	Real-like	No-link
Number	patients	300	300
	visits	2,065	1,939
	patient-years	287	268
	visits per patients	6.9 (3.2)	6.5 (3.3)
Time	follow-up (years)	1.0 (0.5)	0.9 (0.6)
	between visits (months)	2.0 (0.7)	2.0 (0.7)
Observed events (%)	VNI	72 [24.0%]	64 [21.3%]
	Death	28 [9.3%]	24 [8.0%]
ALSFRS _r (baseline)	total	40.6 (3.8)	41.0 (3.8)
	bulbar	10.6 (1.9)	10.7 (1.7)
	fine motor	9.7 (2.0)	9.8 (2.1)
	gross motor	9.1 (2.5)	9.2 (2.4)

Table I6 Comparison of the parameters estimated by the Joint cause-specific Spatiotemporal model with the one of the Longitudinal Spatiotemporel model on the simulated dataset

Legend: Simulated: the value of the parameter used for simulation, Relative difference (%): relative difference between the parameters of the Joint cause-specific Spatiotemporal model and the Longitudinal Spatiotemporel model, Real-like: Real-like simulated dataset (valid shared latent age hypothesis), No-link: No link dataset (invalid shared latent age hypothesis), $\bar{\xi}, \bar{s}, \sigma_s$ parameters are not present as they are fixed by the model ($\bar{\xi} = 0, \bar{s} = 0, \sigma_s = 1$) and $t_0 = \bar{\tau}$

Parameters name			Simulated	Relative difference (%)		
				Real-like	No-link	
Distribution of random effects	Estimated reference time (mean)	t_0	5.000	1.66	1.21	
	Estimated reference time (std)	σ_τ	1.000	-1.79	4.30	
	Individual log-speed factor (std)	σ_ξ	0.790	-2.40	-14.26	
	Curve values at $t_0: \frac{1}{1+g} (g_k)$	g_0	13.958	-12.41	-14.77	
		g_1	5.316	-3.80	15.11	
		g_2	3.993	1.04	16.06	
		g_3	5.704	-3.68	3.42	
	Speed of the logistic curves ($v_{0,k}$)	$v_{0,0}$	0.069	-3.52	-4.59	
		$v_{0,1}$	0.188	-11.81	-23.77	
		$v_{0,2}$	0.198	-15.18	-23.11	
		$v_{0,3}$	0.113	-12.08	-18.60	
	Longitudinal fixed effects	Estimated noises (σ_k)	σ_0	0.066	0.35	0.06
			σ_1	0.076	0.32	0.09
σ_2			0.102	0.19	-0.14	
σ_3			0.036	0.13	-0.19	

Table I7 Comparison of the parameters estimated by the Joint cause-specific Spatiotemporal model with the one estimated by the cause-specific AFT model on simulated data

Legend: , Real-like: Real-like simulated dataset (valid shared latent age hypothesis), No-link: No link dataset (invalid shared latent age hypothesis), NIV: Non Invasive Ventilation initiation, Parameters: parameters of the Weibull distribution with the matched scale (nu for the AFT model and $nu + t_0$ for the joint model with t_0 the estimated reference time), ρ the shape, Joint Spatiotemporal: Joint cause-specific Spatiotemporal model, Cause-specific AFT: Cause-specific Accelerate Failure Time model. Simulated values ($v_1 + t_0, \rho_1$) for both datasets: NIV initiation (7.8, 1.7), death (8.6, 2.8).

		Matched weibull scale	Weibull shape		
		Relative difference (%)	Spatiotemporal (ρ_1)	Cause-specific AFT(ρ_1)	Concordance of hazard progression
Real-like	NIV	-2.75	1.509	4.742 [3.966, 5.671]	yes
	Death	-16.8	3.044	4.954 [3.735, 6.572]	yes
No-link	NIV	133.9	0.527	5.610 [4.649, 6.769]	no
	Death	114.5	0.806	5.147 [3.755, 7.054]	no